分类号_____ 学号 I201121002

学校代码 10487 密级_____

华中科技大学

硕士学位论文

基于穷尽块匹配散斑图案追踪的非接触式脉搏血压测量研究

学位申请人： Hugo Pumacahua Chahuayo

学 科 专 业： 生物医学工程

指 导 教 师： 李鹏程 教授

答 辩 日 期： 2014.10.30

A Dissertation Submitted in Partial Fulfillment of the Requirements
For the Degree of Master of Engineering

Non-contact Measurement of Blood Pulse Pressure using Speckles Pattern Tracking with Exhaustive Search Block Matching Algorithm

Candidate : Hugo Pumacahua Chahuayo
Major : Biomedical Engineering
Supervisor : Prof. Li Pengcheng

Huazhong University of Science and Technology
Wuhan, Hubei 430074, P. R. China

October, 2014

DEDICATION

To GOD

To my Mother in Heaven

To my parents Zósimo and Teodora

To Raphaëlle

独创性声明

本人声明所呈交的学位论文是我个人在导师指导下进行的研究工作及取得的研究成果。尽我所知，除文中已经标明引用的内容外，本论文不包含任何其他个人或集体已经发表或撰写过的研究成果。对本文的研究做出贡献的个人和集体，均已在文中以明确方式标明。本人完全意识到本声明的法律结果由本人承担。

学位论文作者签名：

日期：　　年　　月　　日

学位论文版权使用授权书

本学位论文作者完全了解学校有关保留、使用学位论文的规定，即：学校有权保留并向国家有关部门或机构送交论文的复印件和电子版，允许论文被查阅和借阅。本人授权华中科技大学可以将本学位论文的全部或部分内容编入有关数据库进行检索，可以采用影印、缩印或扫描等复制手段保存和汇编本学位论文。

本论文属于　保密□，　在_____年解密后适用本授权书。
　　不保密□。

（请在以上方框内打“√”）

学位论文作者签名：　　指导教师签名：

日期：　　年　　月　　日　　日期：　　年　　月　　日

摘 要

血压（BPP）和心率(HR)是反映人体生理病理状态的重要的参数，目前血压心率的监测装置主要是基于示波法，心电图法（ECG）以及光电容积脉搏波描记法（PPG）的方法测量，但是这些方法需要通过电极或传感器与病人接触。目前有研究通过一种非接触的光学系统实现血压和心率的远程测量，这种光学测量方法是基于图像互相关的追踪算法实现的，其原理是当激光照射到人的皮肤表面会形成散斑，由于心脏的泵浦会造成皮肤上散斑的变化，通过追踪获取图像上的二次散斑（SSP）的时间变化就可以实现血压和心率的远程测量。

在本文中，我提出使用穷尽块匹配算法（EBMA）,设计了一种非接触光学系统以实现血压和心率的远程测量。同时利用该系统对扬声器进行了模型试验，6 个正常人进行了临床实验；并把测量的结果与传统方法（示波器，血压仪）测得的结果进行对比。在实验中，每次测量时间为 20 秒，然后通过穷尽块匹配算法（EBMA）处理高速相机采集的图像序列；在扬声器实验中，用一串脉冲信号激励扬声器，同时用光学系统提取这串信号的频率和振幅的变化，结果显示我们得到的结果与示波器得到的结果相关系数为 1；在人体实验中，激光直接照射在手腕的动脉上直接提取血压信号，五个受试者在休息时候的结果与传统血压仪的相关性为 0.76，而对于一个运动后的受试者的测量结果显示相关系数高达 0.93。

根据结果显示，该技术是一个实时监测血压的有用工具，甚至未来可以实现对自由行动的人的血压实时监测。这种远程监测血压技术可以对重症监护室的病人进行长期监测，适用于新生儿、处于婴儿猝死综合征的婴儿以及深度烧伤的病人。而且远程检测是完全安全的，特别适合传染病患者使用。

关键词：血液脉冲压　　二次散斑　　穷尽块匹配算法

Abstract

Blood Pulse Pressure (BPP) and Heart Rate (HR) are of primary importance physiological parameters. They are measured using medical monitoring devices based on oscillometric method, electrocardiography (ECG) technique, and photoplethysmography (PPG) method; but they require contact with the patient through electrodes or transducers.

For remote measurements of BPP and HR, a novel non-contact optical system has been implemented in previous works, which is based on tracking temporal changes of the acquired images, associated with the action of mechanical heart pumping, of the reflected secondary speckle patterns (SSP) produced in human skin, when illuminated by a laser beam. In the papers related to this new method, the tracking process was based on correlation algorithm with Matlab. There is a method called exhaustive search block matching algorithm (EBMA) used in communication systems, with good performance and accuracy, so in this work I applied EBMA instead of correlation. I set up and applied this measurement method to a speaker and to six normal people in the laboratory. In parallel the same parameters were measured using conventional instrumentation reference (Oscilloscope, Blood Pressure Monitor) for comparison. A sequence of images was captured, recording them on an average span of 20 seconds; the images were processed using EBMA written in Matlab. Various experiments were performed, for example pulse trains were sent to a speaker and the frequency and amplitude from the vibration were extracted with the optical system, the results showed that the correlation with the results obtained by oscilloscope was 1; BPP also was extracted directly, by illuminating the skin with a laser over the artery in the wrist. For five subjects at rest the results showed that the correlation with the results obtained by blood pressure monitor was 0.76, and for one subject right after exercise the results showed a correlation of 0.93.

According to the results, this technique is a useful tool that can be enhanced and implemented in the near future for real time monitoring of BPP even allowing free movement of the person. So the remote detection could be a valuable tool in intensive care monitoring, long term-monitoring, to use on patients whose conditions can be perturbed or worsened by contact sensors which include neonates, infants at risk of sudden infant death

syndrome, and burn victims, moreover the remote detection complies completely with the safety recommendations concerning risk of electric hazards, valuable in monitoring of contaminated patients.

Key words: Blood Pulse Pressure Secondary Speckle Pattern
Exhaustive Search Block Matching Algorithm.

Abbreviations

AM:	Axial Movement
ASIC:	Application Specific Integrated Circuit
BMA:	Block Matching Algorithm
BPP:	Blood Pulse Pressure
CHD:	Coronary Heart Disease
DBP:	Diastolic Blood Pressure
DBPM:	Digital Blood Pressure Monitor
EBMA:	Exhaustive Search Block Matching Algorithm
ESPI:	Electronic Speckle Pattern Interferometry
FFDDP:	Far Field Downward Displaced Plane
FFFDP:	Far Field Forward Displaced Plane
FT:	Fourier Transform
GC:	Glucose Concentration
HR:	Heart Rate
IF:	In-focus
IR:	Infrared
IU:	Image Unit
MAD:	Mean Absolute Difference
ME:	Motion Estimation
MPPA:	Main Positive Peak Amplitude
MSE:	Mean Square Error
MV:	Motion Vector
ND:	Neutral Density
NSE:	Navier Stokes Equations
OCG:	Optical Cardiogram
PDA:	Pixel Detector Array
PPG:	Photoplethysmography
PSP:	Primary Speckle Pattern
SBP:	Systolic Blood Pressure
SP:	Speckle Pattern
SSP:	Secondary Speckle Pattern
TiM:	Tilting Movement
TrM:	Transversal Movement

目 录

1 Introduction

This work implements an optical technique which is based on the projection of a laser beam on the target and on the tracking the movement of the secondary speckle patterns (SSP) that are created in far field [1]. The speckles are self-interference random patterns; each speckle is a point of reference, and from this point, the phase variations of the scattered light at the surface can be tracked [1], this characteristic has been used in electronic speckle pattern interferometry (ESPI) for measurement of displacement, vibration analysis (amplitudes, slops and vibration modes) and characterization of deformations [2-4]. For deformation object measurements, the speckle pattern (SP) before deformation has occurred (change in load, in temperature, etc.) is subtracted from the pattern after changing has taken place [2]. In this work an imaging camera records the temporal fluctuations and path of SP intensity; in order to apply the EBMA method to the movement of the SPs, the imaging lens was defocused [1]. Now with regard to the sampling frequency of the camera, one of about 500 Hz is sufficient for reconstruction of the QRS heart rate [5-7], nowadays even digital cameras can allow higher sampling [8].

Knowing that cardiovascular diseases are a major cause of death in today's society, measuring vital signs (Blood Pressure and Heart Beat) serves to assess human cardiovascular condition. There are invasive and non-invasive methods for measuring blood pressure, the first method is expensive; by contrast, non-invasive method have become more widely used since they reduce medical costs and they are more easily accepted by patients [9, 10].

Optical sensors are widely used in the diagnosis related to blood pressure and heart rate, they are noninvasive and safe because there is no direct contact with the human body; the cardiovascular pulse generates a change in blood flow amount in the vessels that in turn generates optical power variation which is measured by optical sensor; photoplethysmography (PPG) is the most common measurement method [9]. The PPG monitors the variation (modulation, attenuation) of the reflected light through the tissue (fingertip, earlobe, the forehead, etc.) due to pulsations of the arterial blood; the increasing of blood pressure in the arteries is caused by contract of heart chambers, and a change from diastolic blood pressure (DBP) to systolic blood pressure (SBP) occurs [9]. The difference between SBP and DBP is called blood pulse pressure (BPP) [9, 11, 12]. The BPP can be measured by PPG technique, however skin contact is required and thus it cannot be used for remote measurements; among optical methods for remote measurement there are: optical interferometry, Doppler, image

processing, contactless PPG and ESPI [9].

There are also researches in new methods of remote non-contact measurement of parameters related to the blood pressure such as the method using microwave Doppler radar [13], another method using radio frequency [14], and the method using Pulsed Laser Vibrometer [15, 16].

A system based on the use of SSP was shown to "hear" the heartbeat remotely; the system contains a camera, a lens and a laser source, which illuminates the person's skin, from which speckles are reflected and the SPs are built in the camera's sensor; the lens is slightly out of focus, with this important feature SPs are constant and the vibration of the surface can be converted in 2D displacement (transversal plane) of the speckles, and this displacement can be monitored by an correlation based algorithm in Matlab [1, 2].

In this work, the optical method for remote estimation was experimentally tested to obtain BPP and HR of several people; in the clinical trials, all measurements were performed in a range of about fifty centimeters between the imaging unit and the person's skin; also a speaker was fed with various audio signals in order to measure the frequency and the amplitude of the vibration on the diaphragm.

To estimate the BPP, the temporal frequency and the motion amplitude need to be evaluated, but it is not useful to asses absolute values for several persons; nevertheless, maintaining the angle constant between the laser light and the skin of a particular subject, it is possible to conduct an exhaustive study of signal amplitude. If BPP amplitude increases, the implemented system will get greater amplitude [9].

To estimate motion vectors (MVs) between two or more images from a video sequence with a high level of temporal redundancy, motion estimation (ME) process is used. This is commonly used in object tracking and also in video compression [17-19]. There are various techniques of ME, but only block matching algorithm (BMA) is used for international video compression standards such as MPEG-1, MPEG-2, MPEG-4 and H.264 [20]. BMA begins by dividing the current frame into square blocks, each block is compared with blocks centered at different points within a search window in the previous or reference frame, the distortion is calculated between two blocks, and the point with the lowest distortion is the center for the current block in the reference image; the distortion can be calculated in different ways, including Mean Square Error (MSE) and Mean Absolute Difference (MAD) [21]. Among many developed block matching algorithms, exhaustive search block matching algorithm (EBMA) is the most accurate and computationally expensive algorithm, this algorithm checks all points within search window; there are other algorithms which have tried to

improve the computational complexity of EBMA; some of these algorithms are: New Three Step Search (NTSS), Four Step Search (FSS), Diamond Search (DS), Hexagon-Based Search (HEXBS), Enhanced Hexagon-Based Search (EHEXBS), Pattern-Based Block Motion Estimation (PBME), and Adaptive genetic pattern search algorithm [22]; also other algorithms such as: Hexagon-Diamond Search (HDS) [23], Predictive Motion Vector Field Adaptive Search Technique [24], Multi-stage Interval-based Motion Estimation algorithm (MIME) [25], Multi-Directional Gradient Descent Search (MDGDS) [26, 27], Fast Directional Gradient Descent Search (FDGDS) [26], Cross-Diamond-Hexagonal Search (CDHS) [20], and Directional Gradient Descent Search (DGDS) [28].

In this work, to calculate 2D motion vectors of speckles, in the implementation of the algorithm in MATLAB, the BMA method with the EBMA strategy was used. The block size was chosen as 16x16 pixels and the search range between -16 and 16 pixels in horizontal and vertical direction, and the search criterion was MAD. Unless otherwise specified, the word "movement" means 2D motion.

1.1 Related Work

The system and method for motion detection that I use in this work has been patented by Zeev Zalevsky and Javier Garcia [1].

A. Below I present a summary of that patent:

System components:

Imaging Unit (IU), unit of laser light, and an extraction unit of the vibrations or spatiotemporal paths from the SPs which could be a programmed computer or an application specific integrated circuit (ASIC). The UI consists of a pixel detector array (PDA) and the optical lens. The system features are resolution, pixel size, size of the aperture and focal length. The objective aperture must be large enough to collect several SPs generated on the object. The objective focal length has to be large enough and the pixel size has to be sufficiently small in order to distinguish speckles of the collected SPs. The parameters of IU depend on: the size of the spot of the coherent light on the object, the sampling frequency and the pixel size of the PDA. The spot of coherent illumination can be smaller if the sampling frequency of PDA is higher. In general, the product of these two parameters is higher if the expected speed of movement of the object is higher. The measurement area on PDA pixel has to be bigger if the expected amplitude of the surface movement is higher. If a

PDA with high frame rate is required, then the λ of the light can be made short, i.e., the light can be more visible than infrared light.

The Primary Speckle Pattern (PSP) is generated by the illumination light passing through a diffuser. Secondary Speckle Pattern (SSP) is generated by reflection of the illumination light in a diffuse surface of an object.

The authors analyze the system in the first case when the IU is focused on the object or a small distance from the object. In this case, the image of SP varies randomly with the motion of the object including tilt movement (TiM) and the tracking of the motion through SSP imaging is problematic. The second case that they analyzed is the core and basis of my research, it is when the IU is focused on a plane IF at a remote distance Z_2 of the object (cf. Fig. 2.4), in this case the SSPs generated by the object are dominant and stationary.

The indirect detection of sound and speech is based on optical imaging of SP, useful for TiM; the pattern is formed by illumination of an object by a laser beam. If the focus is on a plane between the object and IU, the plane is called Far Field Downward Displaced Plane (FFDDP); if it is on a plane behind the object, the plane is called Far Field Forward Displaced Plane (FFFDP). The SP associated with the object becomes stationary, then the variation of SP is only displacement, this effect is most evident in FFFDP. The motion can be extracted from the space-time trajectories of the speckles based on motion estimation (ME) techniques as BMA, parametric motion models, optical flow, or pel recursive. It can be separated different sounds produced by a remote source, each sound corresponding to a different region of the PDA from and IU.

In this work I focused the lens on FFFDP.

Following with the summary, the location of the IF plane must meet the condition of far-field approximation (cf. Eq. 2.8). The formation of images of the moving object is associated with vibration, for example vibration from a part in a living body. The movement of regions of an object is determined by their displacements in the first and second image. Each of these regions includes stationary SP.

The motion detection technique can use tracking SP or a region of SP through a number of images (frames). The technique tracks the maximum intensity of the SP, which is determined by the imaging system. For SP tracking, a number of captured speckles by the PDA in each dimension do not have to be very small, and thus it may have correspondence between SPs of different frames. N, the number of speckles captured in a single dimension of the PDA are according Eq. 2.9, it is obtained thanks to the wide divergence of SP making the

lens aperture *A* filled with speckles. The embodiments have different values of *N*: $4 < N < 8$, $8 < N < 10$, $10 < N < 16$, $16 < N < 20$, or $N > 20$. The number of pixels of a PDA in any dimension is greater than *K*x*N*.

General Purpose:

The technique is primarily useful for extracting TiMs, and useful for the detection of movements associated with sounds such as cardiac pulse and the human voice, for the extraction of speech from several people talking at the same time, even from a person in a noisy environment. The SPs are formed by the reflection of infrared coherent light of a human body, particularly the head, cheeks and throat. The sampling rate of the IU is 10 KHz.

Biomedical Applications:

- Detection and monitoring of coronary heart disease (CHD), related to the movement of the left ventricle (LV). CDH generates abnormalities in the motion of the heart's wall. Echocardiography is the most common method of the imaging of beating LV.
- Non-contact detection of heartbeat (HB). The authors showed that the obtained HB was repeatable for the same participant and different from participant to participant.
- The authors coined the term optical cardiogram (OCG), which is like ECG but remotely extracted from the vibration of the human body.
- Formation of biomedical images of a foetus.

Series of experiments:

1) Extraction of sounds from a pair of speakers, IU and object are stationary.
2) Extraction of signals of human voice, singing or shouting, played on a speaker. IU and object are stationary.
3) Speech detection in the throat, face, etc. The person speaks and moves.
4) Simulations for a design of various configurations of detection of speech.
5) Detection of HB in the chest covered with clothes.
6) Pulse Detection of OCG and the Fourier transform (FT) of OCG in the wrist of Subject #1 under physical effort. They obtained an error of 2.25 % and 5.78 % in the calculation of HB compared with a clock polar.
7) Detection of multiple pulses OCG. Subject #2 in rest, 0.14% error. Subject #2 had a

physical effort, error 0.06%. Subject #3 in rest, 0.04% error. Subject #3 under physical effort, 0.00 % error. So this method can be used for non-contact measurement of heart rate (HR).

8) OCG signature detection. OCG Comparison of Subject #4 and #5, the beats from each subject preserves their temporal shape and they are different from each other. The OCGs of subject #6 at rest on different days are similar. OCGs of subjects #7 and #8 have of course different signatures. Therefore the OCG carries a unique signature of a person as fingerprints or retina, then the OCG can be used as key input into security zones. It can even be detected if a person lies since also his OCG will change.

B. Then Zalevsky Zeev et al. [2] made use of the patent [1] and applied it for remote and simultaneous extraction of multiple sources of human speech and heart beat (HB). The authors did some calculations and obtained an F=36mm and K=48. The value of K cannot be very large, since KxN is the region of interest or window on the PDA, and with a high sampling rate that window should be as small as possible.

Experimental results:

The authors, Zalevsky Zeev et al. [2] obtained all the results applying a basic detection algorithm that included **correlation** of unfocused SPs and monitoring the change in peak position. This change in position was the acoustic signal that they managed to extract. There was no post processing for noise removal.

1) Extraction of sounds from a pair of static speakers. The first sound was a pair of fixed frequencies and the second was the cry of a person. The samples were analyzed with the "Specgram" function of Matlab. After processing they obtained the same frequencies.

2) Outdoor Measurements: Reconstruction of the speech signal of a standing or walking subject and illuminating with laser: the back of the head or face. Listening to breathing and HB. The recording of a telephone conversation, and recording through a glass window. Recordings were made at a distance without contact.

3) Measurement of OCG: Results are the same as the ones obtained in the patented Zeev Zalevsky and Javier Garcia invention [1].

Conclusions:

Main advantages of the system are simplicity, modularity, ability to separate various noise sources without the need for sophisticated digital post processing algorithms, and its

usefulness for remote recording of speech even in windy conditions.

C. Yevgeny Biederman et al. [9] applied the invention [1] for remote estimation of BPP through the temporary tracking reflected SSP.

Experimental Setup:

The setup included a green laser and a camera (with slight defocus and connected to a computer) that records reflected SSP from the wrist. The angle of incidence with respect to the skin is 90 °to obtain the smallest spot size; hence the speckle size in the camera was the largest. The spot size is linearly proportional to Z_2 (cf. Fig. 2.4) and inversely proportional to the laser beam's spot diameter (cf. Eq. 2.5). Yevgeny Biederman et al. followed the procedure shown in Fig. 1.1.

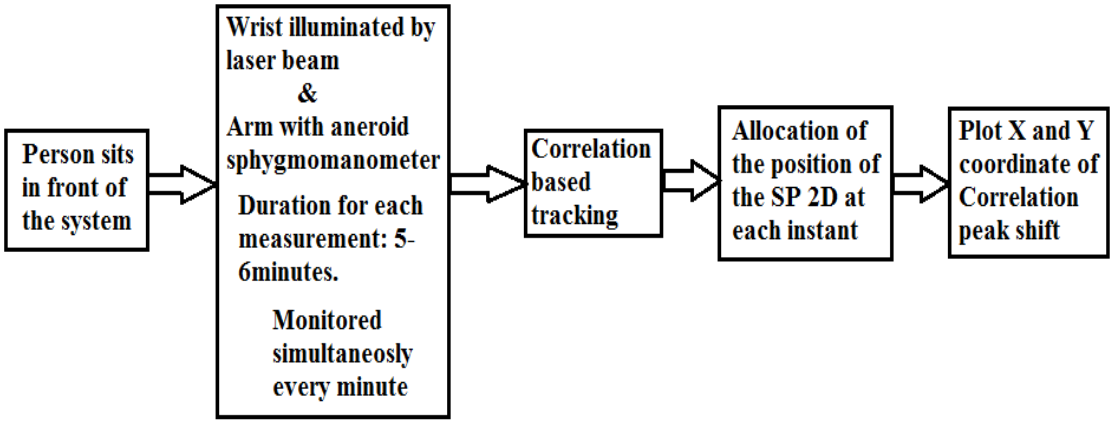

Fig. 1.1 Procedure for obtaining blood pulse pressure (BPP) [9].

The authors obtained a waveform in function of the time, where the peaks and valleys are respectively high and low values; these values were averaged along the measurement time, they got the correlation and the standard deviation or measurement error. They obtained the pulse amplitude of blood pressure (BPP) that corresponds to the relative displacement, in pixel units, of the SP between adjacent video frames. Likewise they obtained the difference (Δ) between SBP and DBP obtained manually with sphygmomanometer. They also calculated the correlation between BPP and the estimated Δ.

Reliability Verification System:

1) Scalability: Remains similar for different subjects (10 subjects). CORR > 0.9 for 9

subjects.

2) Repeatability: Results stable over time. They repeated the measurement in 2 subjects every two months for one year. CORR > 0.9 in both cases.

3) Stability: Constant results for constant pulse pressure. The change for all subjects is less than 15%.

4) Verification Test: In 10 subjects; higher correlation coefficients for BPP, 70% higher than 0.9, 20% between 0.8 and 0.9, 10% less than 0.8; Correlation coefficients for intermediate SBP, 65% greater than 0.9, 35% between 0.8 and 0.9, 5% lower than 0.8; DBP evenly distributed without good statistical property.

5) X axis remained stable at constant conditions and provided the best correlation which was calibrated for each subject in each test.

Yevgeny Biederman et al. [9] concluded that observing the peak amplitude **correlation** it is possible to get a measurement that is proportional to BPP, they state that the method is inexpensive with low power laser, they said that for future works can be the implementation of a multichannel monitoring device of BPP in real time allowing free movement of the subject.

D. Yevgeny Biederman et al. [29] have demonstrated the ability of the invention of Zeev Zalevsky and Javier Garcia [1] to monitor glucose concentration (GC) in the bloodstream, Yevgeny Biederman et al. [29] achieved this by illuminating the wrist with laser and by tracking the temporal changes in the reflected SSP, these changes are produced by the vibration of the skin which is caused by the pulsation of blood flow. Yevgeny Biederman et al. [29] have demonstrated that the temporal shift β which is the relative displacement of the SP is directly proportional to the temporal change of the GC, this change affects the blood viscosity v, which in turn affects the friction between the blood stream and blood vessel walls, and this produces the variation of BPP. The aims of the authors [29] were the analysis of the variation of the temporal pulse profile of TiM by observing the quantitative parameters before and after taking glucose (400 mL of fresh beverage with 40Kcal per subject), and the comparison with a reference value GC obtained by a glucometer. The parameters that they got were classified into two types, those proportional to the change in amplitude and those proportional to the temporal change of the relative displacement of the SP. A parameter which belongs to the amplitude change type was called main positive peak amplitude (MPPA) - which refers to the maximum amplitude for one heartbeat (HB) in pixel units - was the

parameter with better correlation. Yevgeny Biederman et al. [29] used a green laser at 532nm and 10mW, the distance from the IU to hand was 50cm. First the SP was extracted in each frame, then the SP was correlated to obtain the change in the position 2D of the pulse peak versus time, the obtained pulse with mechanical vibration profile was similar to the electrical signal ECG form. The tests were made on four healthy adult subjects. As proof of calibration and stability, the authors illuminated each time exactly the same point on the wrist with laser, and monitored for 30 minutes the subject's hand; so they got results with accuracy of 10-15% of variation.

Yevgeny Biederman et al. [29] said that blood pressure did not change during the experiment, and the change in the pulse profile is only due to the ingestion of glucose. The authors believed that the metabolic process initiated by glucose ingestion generates a cumulative change in the viscosity of the blood. In addition to the correlation coefficient, the authors used the root mean square error (RMSE) to quantify the relationship between the reference data and the estimated data [29].

$$RMSE = \sqrt{\sum_{i=1}^{N} \frac{(x_i - r_i)^2}{N}} \tag{1.1}$$

Where x_i is the i-th sample of the estimated values and r_i is the reference values and N is the number of samples.

Yevgeny Biederman et al. [29] wrote a program in MATLAB to analyze videos and extract the parameters of the files, each file contained 5 seconds of video at 350 fps containing 6 pulses, each pulse was processed separately and the parameters extracted and averaged.

They found no good correlation between the parameters related to temporal change of pulse profile and the change in GC, however the parameters proportional to the change of amplitude have a fairly good agreement with the reference level of GC.

Results:

They showed graphics of the evolution of the MPPA parameter over time versus glucometer baseline. For subject #1 the parameter MPPA showed better correlation. Yevgeny Biederman et al. [29] concluded that there was a high correlation and low error rates, and showed that the amplitude change in the vibration profile of the pulse wave of the wrist was proportional to the change in the positive slope of the GC in the blood.

Future developments:

The authors suggest the implementation of a device with automatic and real-time monitoring, to analyze changes in the GC in the blood while the subject is freely moving.

1.2 Motivation and Contributions

The motivations for the development of this project are based on the importance of non-contact detecting and monitoring of human cardiac activity and blood pressure pulse (BPP). The application of non-contact monitoring can be useful in the following cases:

1. Prolonged monitoring of patients in intensive care unit (premature babies, adults), monitoring at home especially the elderly and other non-clinical areas such as the case of monitoring the health of workers (aircraft pilots, firefighters, etc..) [30].
2. Patients whose conditions may worsen with the use of contact sensors as in newborns, whose skin can be damaged by prolonged use of electrodes in contact with skin [30].
3. Infants with sudden infant death syndrome (SIDS), and in patients with burns [30].
4. The monitoring of contaminated patients or patients in biologically and chemically contaminated environments [30].
5. The BPP is an important indicator of risk of CHD in 60 years persons and older, and is an important prognostic marker of cardiovascular morbidity and mortality. Also detecting high BPP, due to the decrease of the elasticity of arteries, acts as biomarker of the increase of cardiovascular risk and as a risk factor for development of atrial fibrillation [11].

The non-contact monitoring presents the following advantages:

1. No need to apply electrodes or transducers which require precise control or replacement during the monitoring of cardiac activity. No need to apply bracelet in monitoring the BPP, whose continued use may result in discomfort to the patient.
2. Fulfillment of the electrical safety requirements of electro medical equipment.

The main contribution of this work is the use of exhaustive search block matching algorithm (EBMA) as a tool for extraction of the relative movement of the SP of the temporally sequential images in the captured video, instead of using the correlation technique.

1.3 Organization

This work is organized as follows: Chapter 1 presents the current applications of the

method, objectives of the research and the contribution; Chapter 2 presents the system used in this work, also explains the different parts of the model such as hardware and software, and the background of the new measurement method; Chapter 3 describes the motion estimation technique and the EBMA algorithm; Chapter 4 develops the validation of the theoretical algorithm with simulations and provides a comparison between the proposed schemes and other results. The conclusions are summarized in Chapter 5.

2 System Model

2.1 Description of the System

The system that I used to conduct the experiments is shown in the Fig. 2.1. The main and basic components of the measurement system are: Digital camera, Lens, Laser, and a Computer.

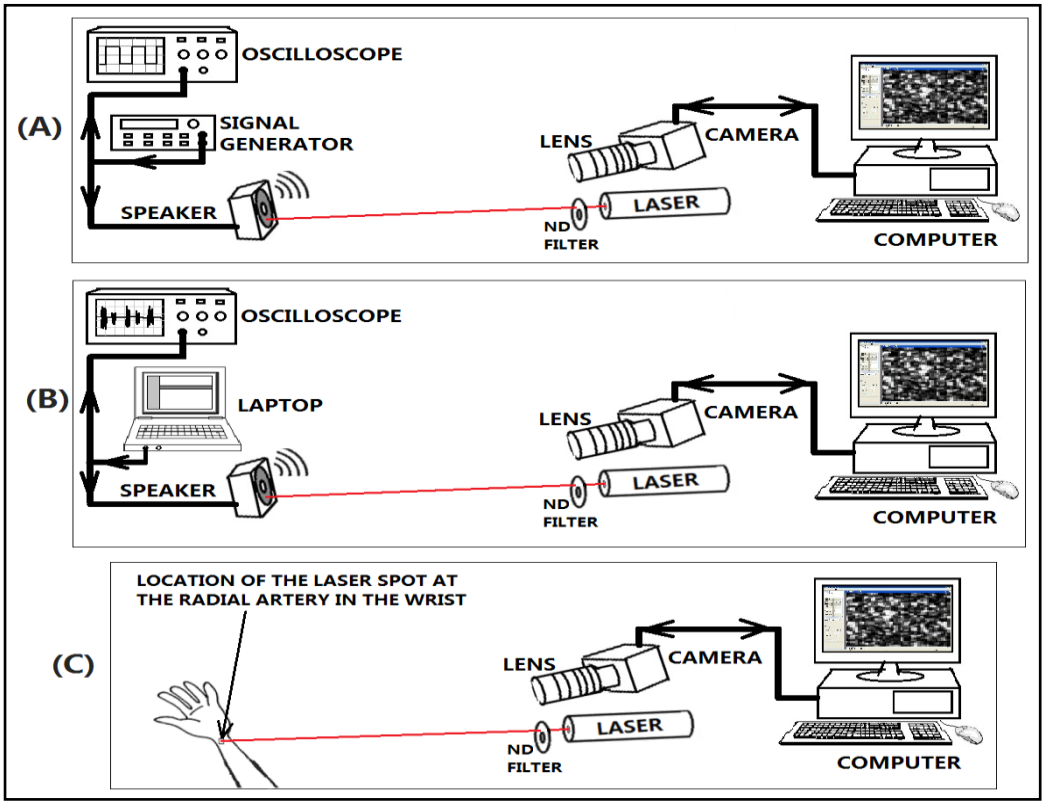

Fig. 2.1 System used to perform the experiments. The System is composed of the Optical System: Imaging Unit (Lens, Camera, Computer), Laser Source (HeNe 632.8nm), Neutral Density (ND) Filter. Also the System is composed of the Oscilloscope Tektronix TDS 1012, Signal Generator SUING TFG2006V, Laptop, and Speaker. In A the source of the periodic pulse train is the Signal Generator, and the Optical System measures the vibration of the diaphragm on the Speaker. In B the Optical System measures the Heart Beat sound on the speaker reproduced by the Laptop. In C the Optical System measures the Blood Pulse Pressure BPP and Heart rate HR on the wrist of the Subject. More details in the following pages.

The Camera is connected to a Computer in which the software of control and the image acquisition card are installed. The Lens is attached to the Camera and its main function is to

focus the SP to be captured from the surface motion or vibration of the object or subject; and the laser is a HeNe type.

The secondary components used are: Oscilloscope, Signal Generator, Speaker, and Laptop. The purpose of using the Oscilloscope is to verify the waveform that is entering into the Speaker, and to compare it to the waveform obtained by the EBMA algorithm. The Signal Generator is used to generate periodic pulse train of different frequencies and voltages (amplitudes). The Speaker is used to simulate an object which surface is vibrating; this vibration corresponds to each different signal and will be illuminated by the laser beam.

In the system the Fig.2.1 (A) and (B) the Speaker is the object, the Fig. 2.1 (C) shows the system used to measure the heart beat and the BPP on the human wrist. The object or the measurement surface is the wrist of a person, from where the Heart Beat (HB) and the BPP will be obtained.

2.2 Imaging Unit (IU)

The Image Unit IU consists in Lens, Camera and Computer. A Tv Zoom Lens was used. This Lens has a Focal Length of F=8-48mm and its maximum aperture is 1:1.0. The brand of the Camera was Optronis (model CL600x2/M) with high resolution and high frame rate, with CMOS sensor of 1280 by 1024 pixels, the pixel size on the detector is 14 by 14 microns i.e. $\Delta x=14\mu m$, which means an area of activity of 17,92 mm by 14,36 mm.

2.3 Laser Source

The Laser source was a HeNe Laser (Class IIIb Laser Product, 15mW maximum at 632.8nm). The ND (Neutral Density) Filter was used to control the intensity of the Laser beam.

2.4 Computer System

The Computer was a desktop type computer; the brand is IEI Technology Corp with a memory RAM of 3.4 GB and CPU @ 3.30 GHz. The operative system is Windows XP. The Computer contains the image acquisition card of the camera Optronis and the software CamSetup for the control of the Camera and the acquisition of the images captured by the Camera. The Computer also contains the software to convert the format of the captured images by the camera for further processing in MATLAB, a program that is also installed in the Computer.

2.5 Image Processing Software: Camsetup, Image Format Converter and Matlab:

Through the software CamSetup can be controlled and set different parameters of the Camera such as: sampling rate (frame rate), size of the image, location of the image, and exposure time among others.

With the software Image Format Converter, the acquired sequence of images can be converted to standard formats like JPEG, it is also possible to visualize that sequence at different speeds, which can help make a preliminary visual analysis of the acquired images.

The version of MATLAB software is R2012a. The implemented algorithm to obtain the HR and the BPP which includes the EBMA algorithm is written and executed in MATLAB. The result is a motion vector graphic of the SP from the previously converted sequence of images as a function on time, graphic corresponding to the heart activity or blood pressure pulse.

2.6 Background

When a rough surface is illuminated by a spatially coherent light, is produced a granular light structure in space, this is known as a speckled pattern (SP) [31]. Also illuminating the surface through a neutral density filter (ND Filter) generates SP. This is the result of self-interference of numerous scattered waves from the surface of a diffusive object; those waves have amplitudes and phases with random variables as shown in Fig. 2.2 [31].

If the object is imaged on the CMOS sensor through a lens, each point from the object contributes to only one point in the image, as shown in Fig. 2.3 [32].

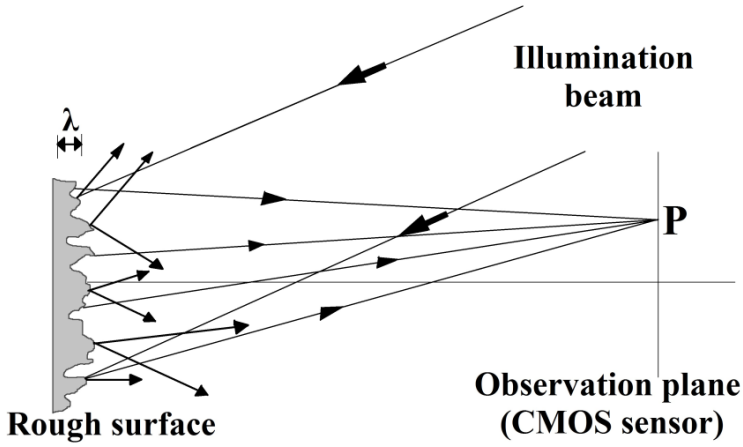

Fig. 2.2 Formation of a speckle pattern [31].

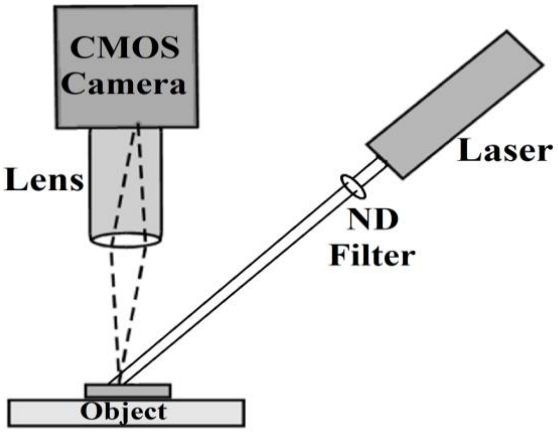

Fig. 2.3 Speckle pattern produced when the object is imaged on the CMOS photo detector through a lens [32].

The size of the area from where the observation plane receives information depends on how defocused is the lens [32].

In the optical system that I use in this work, the lens does not focus on the object, but rather focuses on the far field. As a result, the motion of the object, instead of changing the SP, creates a movement or vibration of a constant SP in the transversal plane, i.e. the same SP is moving. This becomes a very important feature to extract the movement path by tracking the points of maximum intensity [2].

Below, I present a more detailed explanation of the optical system above described. The Fig. 2.4 will be the reference for this theoretical explanation.

Denotations:

(x,y):	Coordinates of the transversal plane.
(x_0 ,y_0):	Coordinates in IF plane.
Z:	Axial axis.
α:	Angle of all rays with respect to Z.
Z_2:	Distance from object to IF plane.
$T_m(x_0 ,y_0)$:	Amplitude of the field distribution of the speckles in the IF plane.
$A_m(x_0 ,y_0)$:	Spatially non-uniform amplitude.
$\psi(x_0 ,y_0)$:	Phase.
ϕ:	Random phase of the speckles.
$I(x_s ,y_s)$:	Intensity of the image in the CMOS sensor.

h:	Spatial impulse response of the Imaging Unit (IU).
(x_s, y_s):	Coordinates in the CMOS sensor plane.
M:	Magnification factor of the lens.
Z_3:	Distance from IU to IF plane.
F:	Focal length of the lens.
β_x, β_y:	Relative shift of SP due to object displacement in the X axe and Y axe.
α_x, α_y:	Tilt angle in the X axe and Y axe.
δ_x:	Resolution or size of the speckle patterns that is obtained at Z_2
λ:	Laser wavelength.
D:	Diameter of the laser spot.
d:	Displacement of SP on CMOS sensor.
Δx:	Size of the pixel in the CMOS sensor.
K:	The minimum number of pixels to see a speckle.
N:	Number of speckles in every dimension of the spot in the sensor.
A:	Diameter of the aperture of the lens.
$F_{\#}$:	Lens F-number.

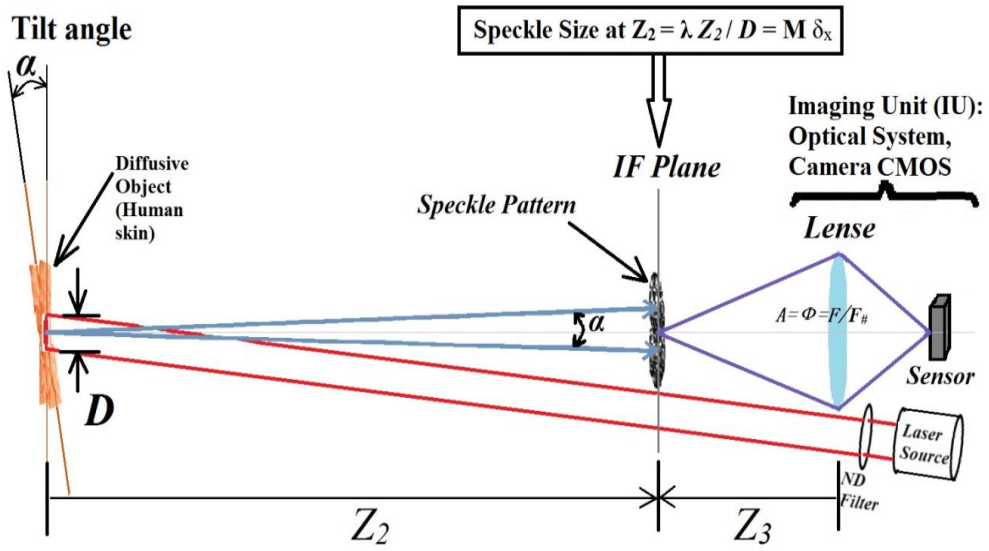

Fig. 2.4 Schematic description of the system [1, 2].

Assumptions:

1. Paraxial or Gaussian approximation, where linear optics or all ray angles are small, angle α of all rays with respect to Z is small enough that $\alpha \approx \sin\alpha \approx \tan\alpha$ [2, 33].
2. The reflectivity over the object's illuminated area is uniform [2].

3. Rigid body (object) movement with three types of movements: Transversal Movement (TrM), Axial Movement (AM) and Tilting Movement (TiM); which cannot be separated and they occur simultaneously [2].

The light, which is reflected on the diffusive object, is captured by a lens onto a CMOS sensor, but the lens is not focused on the object, as is shown in the Fig. 2.4 it is focused on a plane located at a distance Z_2 from the object, that plane is called in-focus (IF) plane and is in the far field approximation. The SPs are formed in the IF plane, those SPs are captured as images by the CMOS sensor in the camera. The surface roughness of the object creates a random phase ϕ, Fresnel integral is used to evaluate the amplitude distribution (T_m) of the speckles performed over ϕ in the Z_2 plane (x_0, y_0) [1, 2]:

$$T_m(x_0, y_0) = \iint \exp[i\phi(x, y)] \exp\left[\frac{-2\pi i}{\lambda Z_2}(xx_0 + yy_0)\right] dxdy = A_m(x_0, y_0) \exp[i\psi(x_0, y_0)] \quad (2.1)$$

Then this amplitude distribution is viewed by CMOS sensor and the captured image has intensity equals to [1, 2]:

$$I(x_s, y_s) = \left| \iint T_m(x_0, y_0) h(x_0 - Mx_s, y_0 - My_s) \right|^2 \quad (2.2)$$

Where h is the spatial response of the impulse, and M is the system magnification inverse, h is calculated in the detector plane (x_s, y_s).

The magnification factor of the lens is [1, 2]:

$$M = \frac{Z_3 - F}{F} \approx \frac{Z_3}{F} \quad (2.3)$$

Where F is the focal length of the lens. In remote measurements, the distance between the object and the lens is typically longer than any other distance implicated in the measurement process ($Z_3 \gg F$).

In the case of TrM, SPs are almost unchanged. The AM does not affect the amplitude distribution. In the case of TiM, this causes displacement of the SPs, as it is shown clearly in Fig. 2.4, and as it can be understood from the following Eq. 2.4 (the linear phase means shift in the far field) [1, 2]:

$$A_m(x_0,y_0)=\left|\iint \exp[i\phi(x,y)]\exp[i(\beta_x x+\beta_y y)]\exp\left[\frac{-2\pi i}{\lambda Z_2}(xx_0+yy_0)\right]dxdy\right| \tag{2.4}$$

$$\beta_x=\frac{4\pi\tan\alpha_x}{\lambda}$$

$$\beta_y=\frac{4\pi\tan\alpha_y}{\lambda}$$

Where β_x and β_y are the relative shift of SP due to motion of the object and the angles α_x and α_y are the tilt angle in the X and Y axes respectively. TrM, AM and TiM are not separated, but TrM and AM produce insignificant changes in the imaged SP, then the overall effect of those three movements is just pure shift that can be easily detected by the EBMA. The size of the SPs obtained in the Z_2 plane and imaged at the CMOS sensor plane is equal to [1, 2]:

$$\delta_x=\frac{\lambda Z_2}{D}\cdot\frac{1}{M}=\frac{\lambda F}{D}\cdot\frac{Z_2}{Z_3} \tag{2.5}$$

The displacement (d) of a SP on the CMOS sensor of the camera is as follows [1, 2]:

$$d=\frac{Z_2\alpha}{M}=\frac{Z_2F}{Z_3}\alpha \tag{2.6}$$

Supposing that Δx is the size of the pixel in the CMOS sensor and that every speckle in the sensor plane will be seen at least by K pixels, which means $\delta_x = K\Delta x$, then the requirement for the focal length is [1, 2]:

$$F=\frac{K\Delta x Z_3 D}{Z_2\lambda} \tag{2.7}$$

Another requirement is that Z_2 has to fulfill the far field approximation which is [1, 2]:

$$Z_2>\frac{D^2}{4\lambda} \tag{2.8}$$

The number of speckles in every dimension of the spot equals to [1, 2]:

$$N=\frac{A}{M\delta_x}=\frac{AD}{\lambda Z_2}=\frac{F\cdot D}{F_{\#}\lambda Z_2} \tag{2.9}$$

Where A is lens aperture diameter, $F_{\#}$ is lens F-number, $M\delta_x$ is SP size obtained at Z_2

plane.

Below, I will explain the mathematical background of blood pressure measurement.

Denotations:

Q: Blood flow.

ΔP: Pressure drop across the vessel.

R: Inner radius of the vessel in diastole.

L: Length of the blood vessel.

v: Blood viscosity.

r: Radial axe in cylinder coordinates.

x: Longitudinal axe in cylinder coordinates.

P: Pressure in cylinder coordinates along the *r* and *x*.

ρ: Blood density.

w: Longitudinal velocity of the blood fluid in *x* direction.

u: Radial velocity of the blood fluid in *r* direction.

v_r: Velocity of the radial expansion of the vessel.

C_a: Elastic properties of the arterial wall.

P_d: Change in the blood pressure (systolic minus diastolic).

d*r*: Radial displacement of the blood vessel.

v_f: Blood flow longitudinal speed at a point on a streamline.

g: Gravity acceleration.

z: Elevation of the point above a reference plane

C: An arbitrary constant.

f: Force which is perpendicular to the cross section of the vessel.

a: Unit area of the arterial vessel.

dP: Change in blood pressure.

E: Elastic modulus of the vessel wall.

β: Relative shift of SP due to object displacement.

α: Angle of tilting of the object

K_1: Linear function of λ.

The commonly known as the Poiseuille equation can be used to better approximate the factors that influence blood flow through a cylindrical vessel (cf. Fig. 2.5) [9, 34]:

$$Q = \frac{\Delta P \pi R^4}{8 \nu L} \tag{2.10}$$

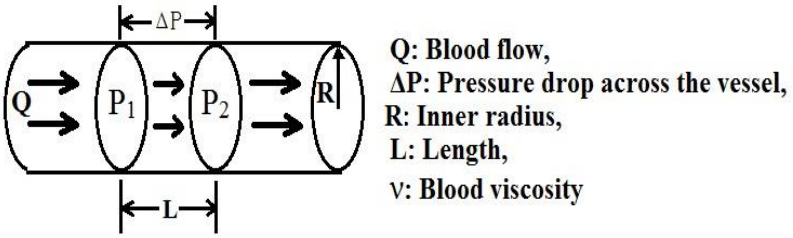

Fig. 2.5 Cylindrical blood vessel [34].

To model the radial change in a blood vessel, Yevgeny Beiderman et al. [9] described two mathematical models:

1st Mathematical Model, Navier Stokes Equations (NSE) [9]:

$$-\frac{dP}{dx} = \underbrace{\rho\left(\frac{dw}{dt} + u\frac{dw}{dr} + w\frac{dw}{dr}\right)}_{\text{Inertial Forces}} - \underbrace{\nu\left(\frac{d^2w}{dr} + \frac{1}{r}\frac{dw}{dr} + \frac{d^2w}{dx^2}\right)}_{\text{Viscous Forces}} \tag{2.11}$$

$$-\frac{dP}{dr} = \overbrace{\rho\left(\frac{du}{dt} + u\frac{du}{dr} + w\frac{du}{dx}\right)} - \overbrace{\nu\left(\frac{d^2u}{dr^2} + \frac{1}{r}\frac{du}{dx^2} + \frac{d^2u}{dx^2} + \frac{u}{r^2}\right)} \tag{2.12}$$

$$\frac{du}{dr} + \frac{u}{r} + \frac{dw}{dx} = 0 \tag{2.13}$$

Where r and x are respectively the radial and longitudinal axes in cylinder coordinates, P is the pressure along r and x, ρ is the blood density, w is the blood longitudinal velocity, and u is the blood radial velocity [9].

In Eqs. 2.11 and 2.12, inertial forces minus viscous forces result in a pressure drop per unit length, and Eq. 2.13 shows a continuity equation. The blood vessel's radial expansion velocity υ_r was derived from NSE [9]:

$$\upsilon_r = RC_\alpha \frac{P_d}{dt} \tag{2.14}$$

In this case, R is the vessel's radius in diastolic blood pressure (DBP), C_α symbolizes

arterial wall elastic properties and P_d is the blood pressure variation. Integrating with respect to time the Eq. 2.14 [9]:

$$dr = RC_{\alpha}P_d \tag{2.15}$$

The previous Eq. 2.15 shows that the **blood vessel's radial displacement d*r* is linearly dependent on the blood pressure difference**.

2nd Mathematical Model, Bernoulli's law (cf. denotations in the previous two pages for the meaning of the variables and constants) [9]:

$$\underbrace{\frac{1}{2}\rho v_f^{\,2}}_{\text{Dynamic pressure}} + \underbrace{\rho g z}_{\text{Static pressure}} + P = C \tag{2.16}$$

Where P is the pressure at the point.

Pressure losses in the direction of the flow generate a force *f* that equals to:

$$f = -adP \tag{2.17}$$

Where *f* causes radial extraction of the vessel. Applying the second law of Newton on Eq. 2.17 is obtained:

$$-a\frac{dP}{dx}dx = \frac{dv_f}{dt}\rho a dx \tag{2.18}$$

Or:

$$\frac{dP}{dx} = \rho\frac{dv_f}{dt} \tag{2.19}$$

A solution for the extraction of a relative radial displacement (d*r*) of a vessel is given by [9]:

$$dr \approx \frac{R}{E}dP \tag{2.20}$$

As in Eq. 2.15 the Eq. 2.20 shows that **the relative radial displacement of the blood**

vessel is linearly dependent on its pressure difference [9].

According to the Eq. 2.4 a relative displacement of the SP is [9]:

$$\left.\begin{aligned} \beta = \frac{4\pi \tan\alpha}{\lambda} \approx \frac{4\pi\alpha}{\lambda} \rightarrow \alpha \approx K_1\beta \\ K_1 = \frac{\lambda}{4\pi} \end{aligned}\right\} \tag{2.21}$$

Using basic theory of geometry and the paraxial approximation, as it is shown in the Fig. 2.6, it can be said that **the radial displacement of the blood vessel is proportional to the tilt angle**:

$$dr \approx \alpha \tag{2.22}$$

From Equations 2.20, 2.21 and 2.22 is obtained:

$$dP \approx \frac{E\lambda}{4\pi r}\beta \tag{2.23}$$

This means that **the change in blood pulse pressure (BPP) is linearly proportional to the relative shift of the speckle pattern**.

So when a self-interference pattern is observed, detected and constructed on the CMOS sensor plane by the camera, a pattern temporal change between two adjacent frames is connected to a relative spatial shift [9]. Using exhaustive search block matching algorithm (EBMA) estimation movement, it is possible to extract the relative shift of the SP, therefore can be extracted the BPP.

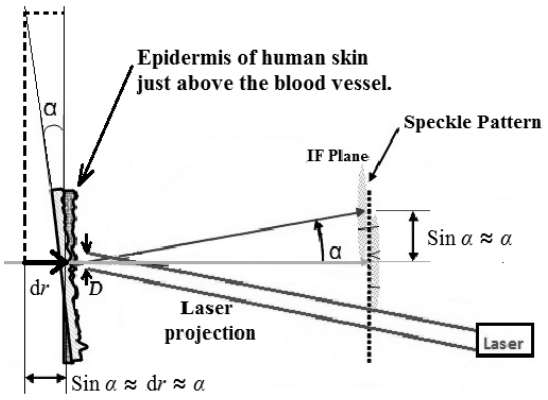

Fig. 2.6 Schematic description of the relation between the shift of the SP and the radial displacement of the blood vessel.

In order to calculate the alpha angle (α) of the tilting movement, the alpha angle from the Eq. 2.6 is isolated as follows:

$$\alpha = \underbrace{\frac{Z_2 F}{Z_3 d}}_{radians} = \underbrace{\frac{Z_2 F}{Z_3 d} \times \frac{180}{\pi}}_{\text{deg}rees} \tag{2.24}$$

Where d is the displacement of the SP obtained by the optical system, in this work usually the displacement is in the order of micrometers and the alpha angle less than one sexagesimal degree.

2.7 Summary

In the first place the surface of interest has to be illuminated by the Laser Beam. Then the Camera has to be focused through the Lens system, not on the surface of interest, but in the Far Field Forward Displaced Plane (FFFDP) behind the object of interest (wrist), so that the displacement of SP, which is invariable, as a result of the vibration of the object of interest, can be seen on the Computer screen. The acquired images by the Camera are stored in real time via the acquisition hardware and software, then the format is converted to JPEG or other standard formats so that they can be read by MATLAB. Then the sequences of images are processed through the EBMA algorithm written and executed in MATLAB. Finally the graphic of the cardiac activity or blood pressure pulse is obtained for analysis and comparison.

3 Key Technologies and Applied Algorithm

3.1 2D Motion Estimation:

Two Dimensional (2D) motion estimation (ME) is part of the video processing system and has many applications such as: calculating of motion vector (MV), video compression, video filtering, etc. In video compression, the estimated MVs are used to generate a frame which is motion-compensated and this is the result of the codification of a previously reference frame. The final purpose is to reduce as much as possible the total bits used for encoding the MVs and the prediction errors. The variation over time of the intensities of the image is the base of ME algorithms.

3.1.1 General Methodology of Motion Estimation:

Suppose two frames $\Psi(x, y, t1)$ and $\Psi(x, y, t2)$. The MV in x (cf. Fig. 3.1) between times t_1 and t_2 is the displacement of point t_1 to point t_2. The frame at t_1 is the current or anchor frame, and the tracked or target frame is at t_2, the current frame can be before or after the tracked frame over time. In the Figure 3.1, when $t_1 < t_2$ is forward motion estimation and when $t_1 > t_2$ is backward motion estimation.

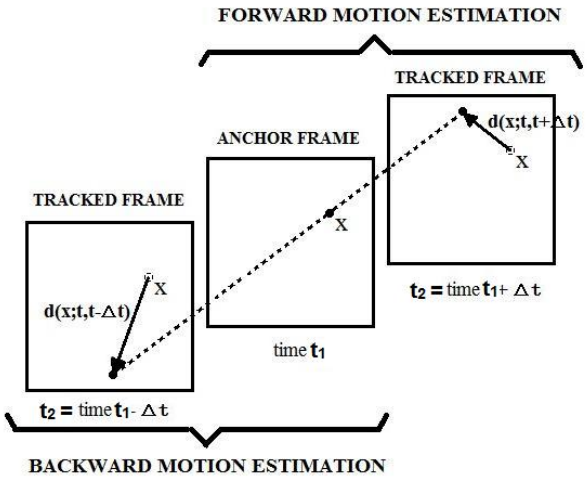

Fig. 3.1 Forward and backward motion estimation [35].

In this work I used Backward Motion Estimation.

Let Ψ_1 (**x**) and Ψ_2 (**x**) be reference frames and tracked frames, respectively. The motion field is **d**(**x; a**), where the vector **a** = $[a_1, a_2, ..., a_L]^T$ contains all motion parameters. **w**(**x; a**) = **x** + **d**(**x; a**) is the mapping function, the goal is to calculate **a** [35].

The method that I used in this work is based on the constant intensity assumption and on three key stages which are:

A. PARAMETERIZATION OF THE UNDERLYING FIELD MOVEMENT:

A simple model is the partition of the image into small blocks as shown in Fig 3.2. The simplest version models the movement in each block by a constant translation, and then the goal of the estimation is to find an MV for each block.

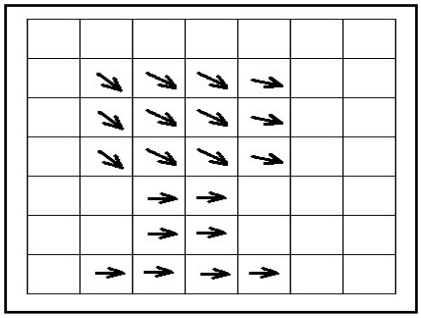

Fig. 3.2 Motion representation based on blocks [35].

B. CRITERIA FOR MOTION ESTIMATION:

This criterion is based on the difference of the displacement of the frame and minimizes the sum of errors between luminance values of each pair of corresponding points between the current frame Ψ_1(**x**) and the tracked frame Ψ_2(**x**). It is known that **x** in Ψ_1(**x**) moves to **w**(**x**; **a**) in Ψ_2(**x**). The criterion function expressing the above can be written as [35]:

$$E_{DFD}(\mathbf{a}) = \sum_{X \in \Lambda} \left| \Psi_2(\mathbf{w}(\mathbf{x};\mathbf{a})) - \Psi_1(\mathbf{x}) \right|^p \tag{3.1}$$

Where Λ is the domain of all pixels in the current frame Ψ_1, and p is a positive number. The Eq. 3.1 is called mean absolute difference (MAD) when p = 1, and it is called mean square error (MSE) when p = 2. The error of image, e (**x**; a) =Ψ_2(**w**(**x**; **a**))$^-$ Ψ_1(**x**), is usually called displaced frame difference (DFD) image, then the Eq. 3.1 measures the DFD error and when its gradient fades, it is possible to minimize DFD.

C. LOOKING FOR THE OPTIMAL PARAMETERS OR MINIMIZATION METHOD:

With the use of MAD in the method of exhaustive search block matching algorithm (EBMA), which will be reviewed below, it is possible to minimize the error function (cf. Eq. 3.1) and thus achieve the global minimum.

3.2 Block Matching Algorithm (BMA):

BMA consists in dividing the image into non-overlapping blocks, and in assuming that the motion in each block can be described by a simple parametric model. Let B_m be the image which represents the m-th block in the image, and Let M be the number of blocks, then $\boldsymbol{M}$ = 1, 2, ..., M. The division into blocks satisfies the following expression [35]:

$$\bigcup_{m \in M} B_m = \Lambda, \; and \; B_m \bigcap B_m = \varnothing, m \neq n \tag{3.2}$$

The block is of square shape and the motion of each block is assumed constant, i.e. the whole block is subjected to a translation, this is called block-wise translational model [35]. Thus, the goal of the motion estimation is simply to find the MV for each block, or estimate the displacement under a measurement error. The displacement that minimizes the error is considered to be the MV of the image.

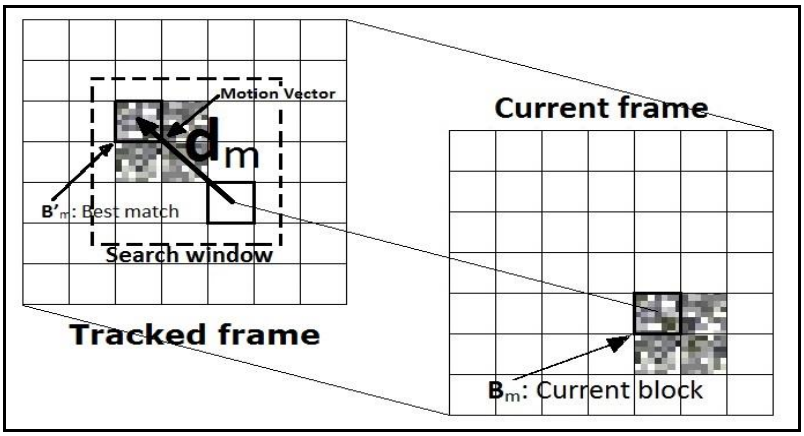

Fig. 3.3 Basic diagram of block matching algorithm [35].

As shown in the previous Fig. 3.3, the blocks of the current frame are compared with the blocks of the tracked frame (before the current), this comparison is made by sliding the current block over a particular area of pixels (search window) of the tracked frame. Then using a criterion it is possible to find the block with the highest similarity (or with the minimum measured error) among the candidates within the fixed search window of the tracked frame. If the selected block is not in the same position in both frames, it means that it has moved. The

distance of the block which coincides in the tracked block with the block in the current frame is defined as the estimated MV, and this will be assigned to all the pixels of the block.

The desirable requirements for a good BMA are: convergence, few search points, few iterations, and immunity to noise. Besides, there are other important criteria such as hardware complexity.

3.3 The Exhaustive Search Block Matching Algorithm (EBMA):

Let B'_m be the block to be found in the tracked frame that corresponds to the block B_m in the current frame. These two blocks are compared and a minimum error is estimated between them, then the estimated MV from block B_m becomes the vector displacement $\mathbf{d}_m$ between the spatial positions of B'_m and B_m. According to block-wise translational model mentioned above, $\mathbf{w}(\mathbf{x}; \mathbf{a}) = \mathbf{x} + \mathbf{d}_m$; $\mathbf{x} \in \boldsymbol{B}_m$, the Eq. 2.1 can be written as [35]:

$$E(\mathbf{d_m}, \forall m \in M) = \sum_{m \in M} \sum_{X \in B_m} \left| \Psi_2(\mathbf{x}+\mathbf{d_m}) - \Psi_1(\mathbf{x}) \right|^p \tag{3.3}$$

Since the estimated MV for a block is independent from other blocks, it is possible to estimate the MV for each block individually. The minimization of the accumulated error along this block only can be written as [35]:

$$E_m(\mathbf{d_m}) = \sum_{X \in B_m} \left| \Psi_2(\mathbf{x}+\mathbf{d_m}) - \Psi_1(\mathbf{x}) \right|^p \tag{3.4}$$

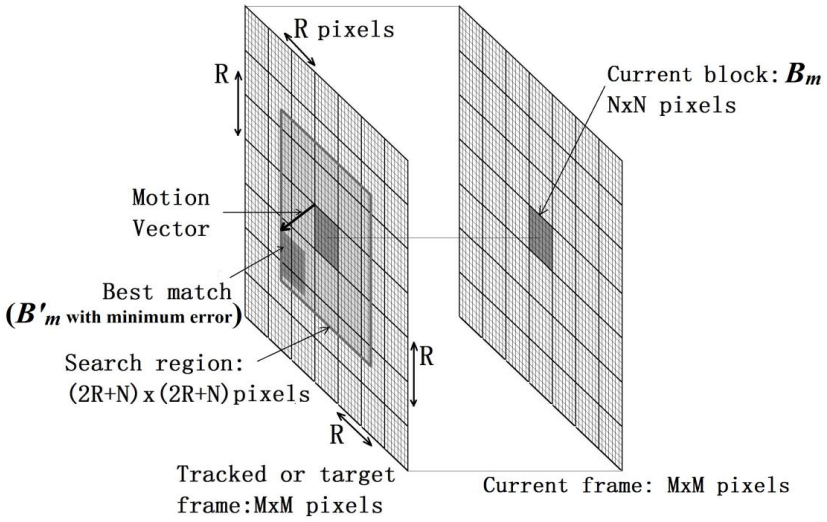

Fig. 3.4 Search procedure of exhaustive search block matching algorithm (EBMA) [35].

Using a method called *exhaustive search block matching algorithm* (EBMA), it is possible to find a $\mathbf{d}_m$ that minimizes the error (cf. Eq. 3.4). As shown in the previous Fig 3.4

the EBMA allows to calculate the optimal $\mathbf{d}_m$ for B_m making comparison with all the candidate blocks B'_m in the tracked frame in a predefined search region, and then allows to find the block with a minimal error.

In order to reduce the computational load, the MAD error will be used, i.e. p=1. There is symmetry in the search region regarding the current block B_m, till R pixels to the left, right, above and below, as illustrated in Fig. 3.4. The accuracy of the estimation depends on the size of the search step which is the distance between two adjacent candidate blocks in the horizontal or vertical direction of the search window in the tracked frame. Along both directions is used the same step size.

Let M x M be the size of the image or frame in pixels, let N x N be the block size in pixels, let ± R be the search range in pixels (cf. Fig 3.4), and the step size is equal to one pixel, then:

- $(2R+1)^2$ = Total number of candidate blocks for the corresponding matching in the tracking frame for each block in the reference frame.
- N^2 = Number of operations for calculating MAD of each estimated candidate.
- $(2R+1)^2 N^2$ = Number of operations for estimating the MV of a block.
- $(M / N)^2$ = Number of blocks (assuming that M is a multiple of N) in an image.
- $M^2(2R+1)^2$ = Total number of operations for a full frame, and is independent of N.

3.4 Applied Algorithm:

The applied algorithm which includes EBMA in this work was written in MATLAB. In the Fig. 3.5 the flowchart shows the major steps in EBMA. Basically two frames belonging to the vibration of the surface illuminated by the laser are continuously compared.

The EBMA applied is an adaptation of the EBMA for compensation of images made by Aroh Barjatya [21], on which I added the instructions for reading the sequences of images obtained by the camera Optronis and stored by its respective card acquisition. I have also added the method of calculating the average and spectrum of the motion vector MV [36], and the procedure to plot the MV with respect to time. Besides, I wrote the procedure for the calculation of the total average displacement of the SP. Since the displacement of the SPs in the focus plane has components in the X and Y axes, then I have also added a procedure to calculate the resulting MV equivalent to the square root of the sum of the squares of the components X and Y; so the resulting MV is plotted over time, which became the OCG.

Also during the process, the algorithm took the first ten pulses from the obtained OCG and calculated for each period of the OCG (which indeed includes one pulse) the SP

displacement in pixels which is the subtraction between the maximum positive value and the minimum negative value, then the "equivalent" value to BPP was the average of the ten SP displacements.

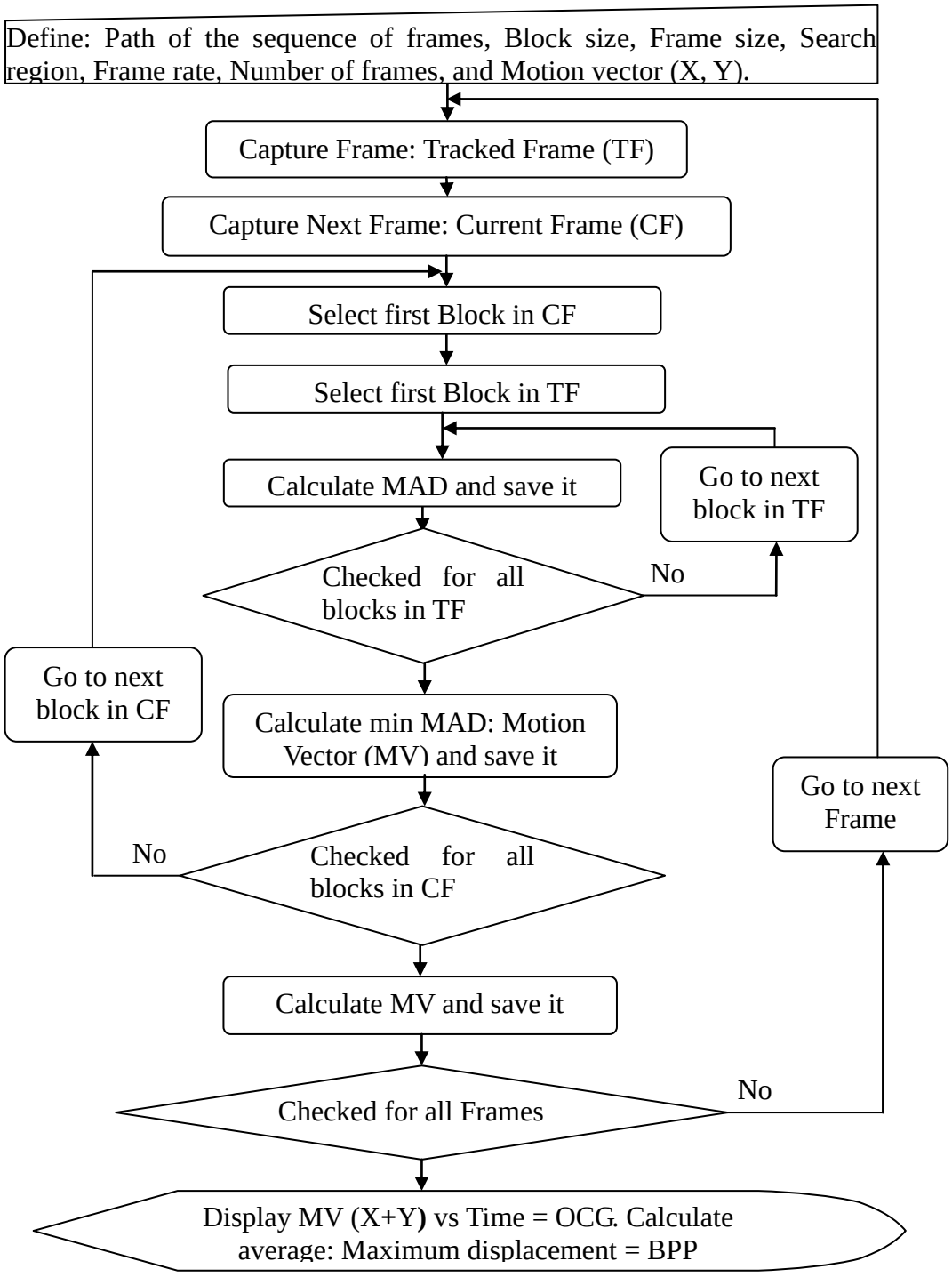

Fig. 3.5 Flow chart showing the steps for EBMA. MDA: mean absolute difference, OCG: Optical Cardiogram, BPP: Blood Pulse Pressure [37].

4 Experiments and Results

First I had to properly focus, in the Lens/Camera, the image of the Laser beam on the speaker to get a good image of Speckle Patterns (SPs). The size of the image was 64x64 pixels. The Fig. 4.1 shows the typical image of the SPs acquired by the Lens/Camera.

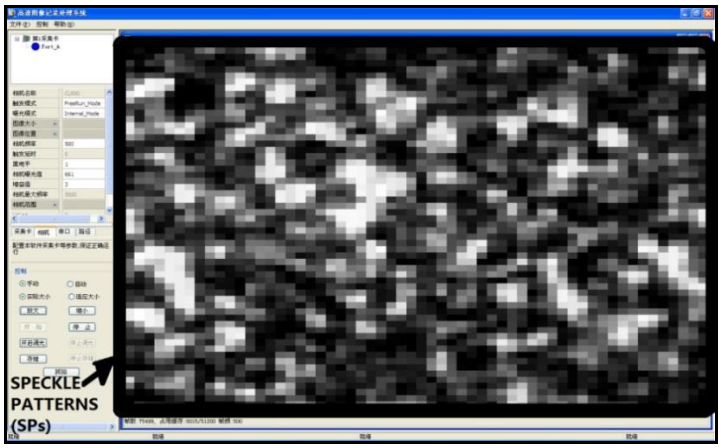

Fig. 4.1 A real-time image, as it is seen on the Computer screen, of the SPs which are taken by the Lens and the Camera, the image size is 64x64 pixels.

4.1 First Experiment: Measurement of Pulse Train on Speaker

The Fig. 4.2 shows the configuration which was used in this first experiment.

One speaker was used as the subject, the distance from the camera/laser to the Speaker was 50cm, and one Signal Generator was used to apply the signal to the Speaker, the Oscilloscope was used as a reference measurement and verification of the shape, amplitude and frequency of those signals.

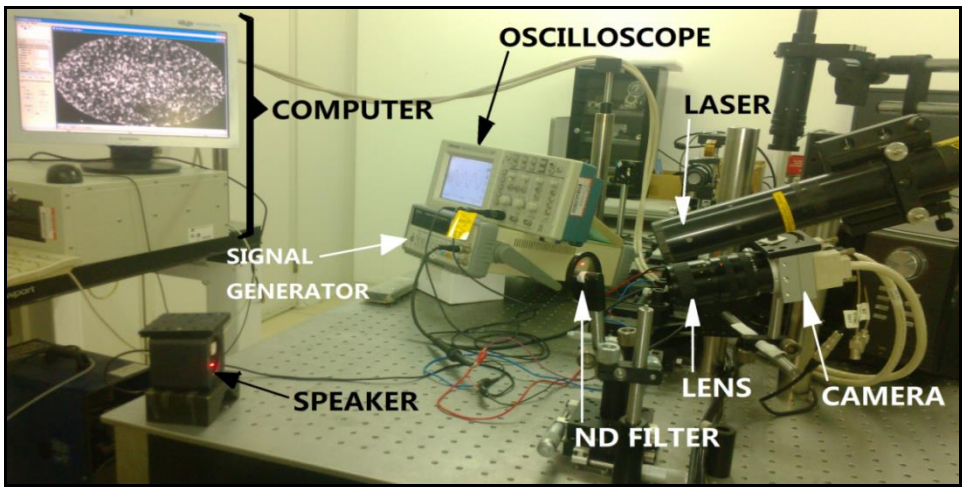

Fig. 4.2 Configuration of the system for remote measurement of the vibration on the Speaker

The speaker converts the applied electric signal into physical vibration on the surface of its membrane; this vibration becomes SP displacement after illuminating that surface with laser, and with the optical method and EBMA it is possible to get the tilt movement of the membrane i.e. to get the same waveform applied to the Speaker. In this experiment was used a periodic pulse train as electric signal, its amplitude and frequency were changed.

4.1.1 Frequency Variation:

The exposure time was 700 us, and the frame rate was 20 fps. The focal length was 48 mm, the focus was 10 m, and the aperture was 1.25. The power of the Laser on the speaker was around 3.62 mW. In the Signal generator the periodic pulse train had 1Vpp and its frequency varied from 0.7Hz to 2.5Hz, so seven different signals were sent to the Speaker, besides the pulse width was one fifth of the period T (Fig. 4.3 (A)).

The following table 4.1 shows the reference measurement (Oscilloscope) and the measurements obtained from the Optical System and the EBMA.

Table 4.1 Frequency measured by reference oscilloscope and EBMA method

Frequency Signal Generator (Hz)	Measured Frequency by Oscilloscope (Hz)	Measured Frequency by Optical Method (Hz)	Measured Pulse Width by Oscilloscope (ms)	Measured Pulse Width by Optical Method (ms)
0.7	0.7042	0.7	280	325
1	1	1	200	225
1.3	1.316	1.35	160	150
1.6	1.667	1.65	130	150
1.9	1.923	1.95	110	100
2.2	2.222	2.2	90	100
2.5	2.5	2.5	80	100

In the Fig. 4.3 (A), (B) it is shown one of those seven signals, and (C), (D) are the comparison of all the seven signals, and shows that the Correlation in both cases is almost 1. From (A) and (B), the voltage peak to peak (Vpp) corresponds to a displacement of 16 pixels in the sensor of the Camera.

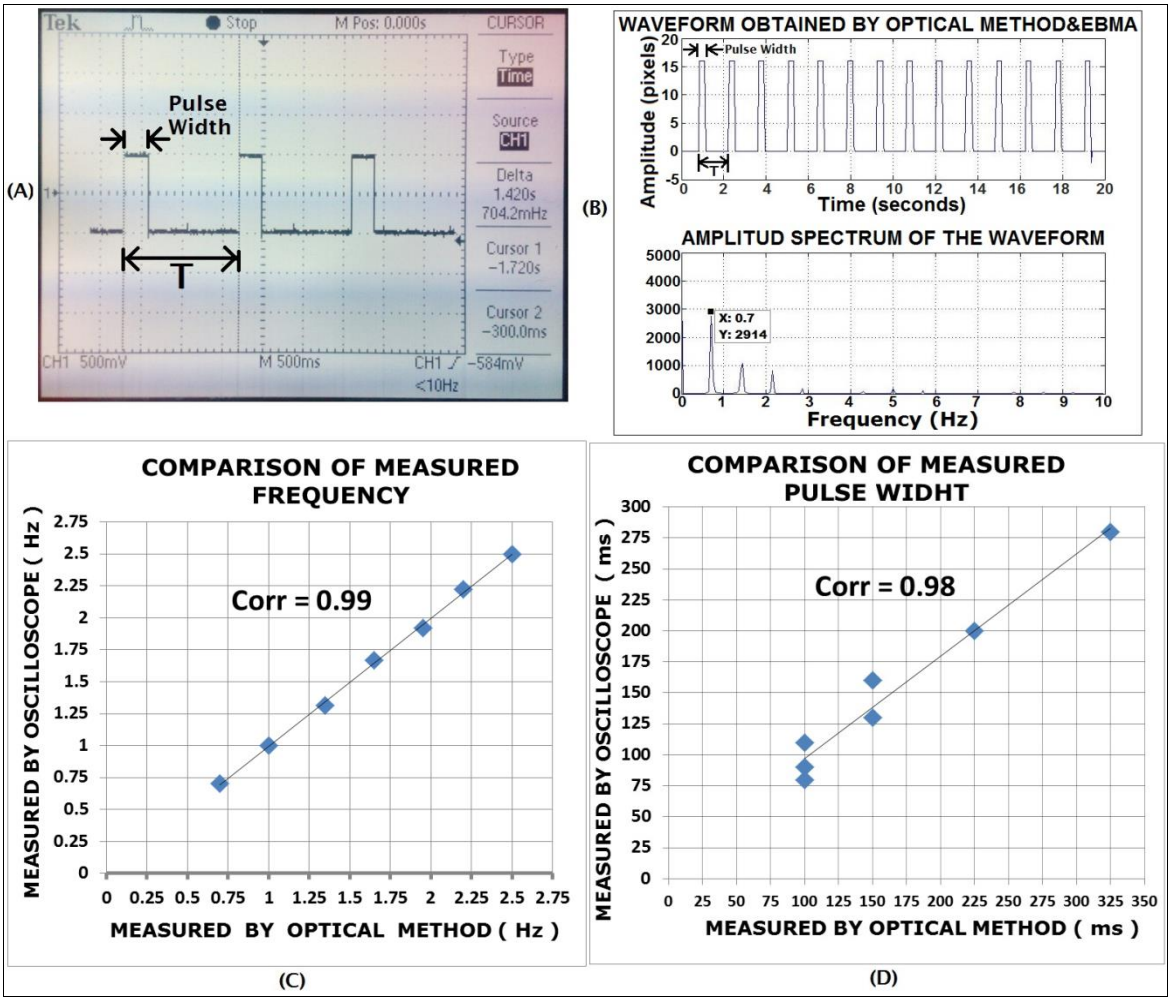

Fig. 4.3 (A): Oscilloscope display of one of the seven signals sent to the Speaker from the Signal Generator, in this case is a 1Vpp and 0.7Hz pulse train (B): Temporal plot of the outcome from the Optical System and EBMA, in this case 16 pixels is equal to 1Vpp. In the spectrum plot 0.7Hz is the main frequency and the others are the harmonics. (C) and (D): Comparison between Optical Method and the reference, (C) Frequency and (D) Pulse width, in both cases Corr≈1.

4.1.2 Amplitude Variation

The exposure time was 700 us, and the frame rate was 20 fps. The amplitude was changed in the signal generator from 1Vpp to 0.1Vpp, but the frequency was constant equal to 1 Hz. To equal 1 Vpp at a total displacement of 10 pixels of the SP in the Camera sensor, the Focus was 1m, the aperture was 1, and focal length was 30 mm. The power of the Laser on the speaker was around 1.7 mW. The table 4.2 shows the results:

Table 4.2 Amplitude measured by reference Oscilloscope and EBMA method.

Selected peak to peak amplitudes in the Signal Generator (Vpp)	Measured Peak to peak voltage amplitude by Oscilloscope (Vpp)	Obtained SP displacement amplitude by Optical method and EBMA (pixels)
1	1	10
0.9	0.904	9
0.8	0.8	8
0.7	0.704	7
0.6	0.6	6
0.5	0.504	5
0.4	0.4	4
0.3	0.304	3
0.2	0.2	2
0.1	0.1	1

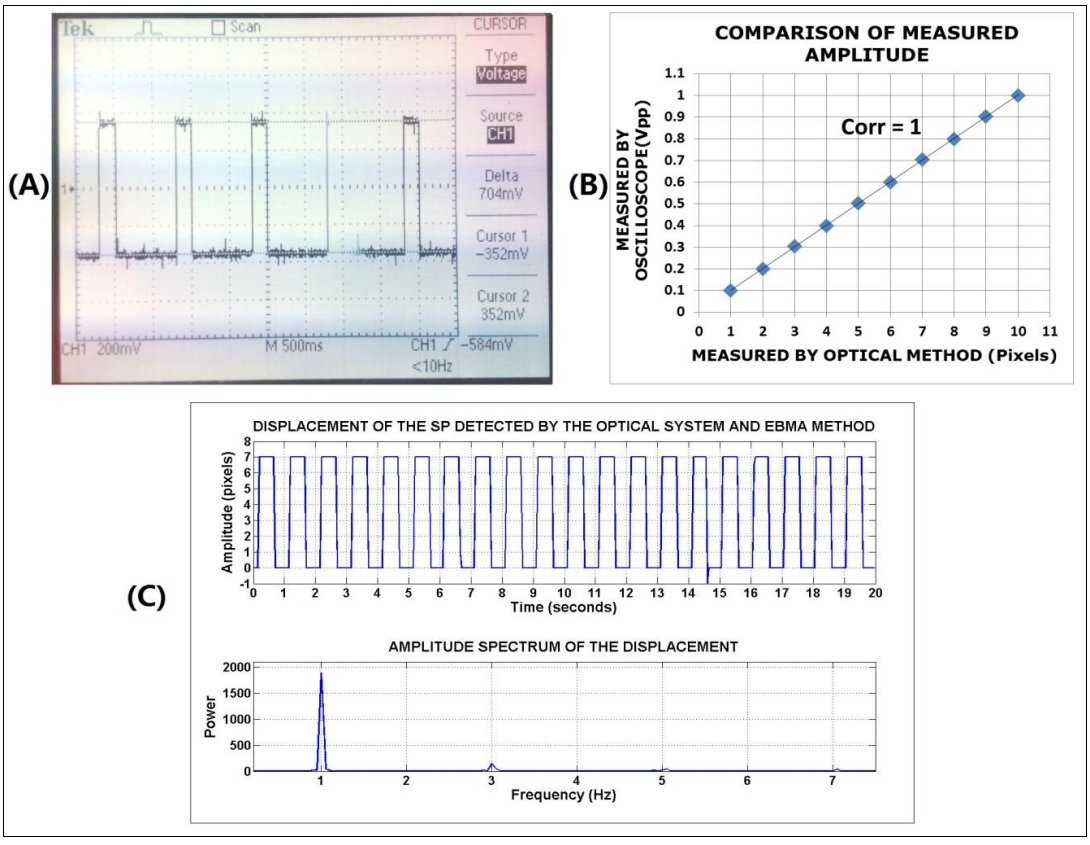

Fig. 4.4 (A): Oscilloscope display of one of the seven signals sent to the Speaker from the Signal Generator, in this case it is a 0.7Vpp and 1Hz pulse train. (B): Comparison between Optical Method and the reference, Corr=1. (C): Temporal plot of the outcome from the Optical System and EBMA method, in this case 7 pixels is equal to 0.7Vpp. In the spectrum plot 1Hz is the main frequency.

For this experiment of amplitude variation, the correlation between the Optical System used in this work and the reference system (Oscilloscope) was 1. The comparison of the two systems is shown in Fig. 4.4(B); furthermore this figure shows one of the ten periodic pulse trains on the Oscilloscope, as it is sent to the Speaker, and the corresponding waveform obtained by the optical system and method EBMA. However, in this case the method EBMA did not provide a good measure of the pulse width; instead the Fig. 4.4(C) shows a square wave.

4.2 Second Experiment: Measurement of Heart Beat Sound on Speaker

The results of this experiment are shown in the following Fig. 4.5 and Fig. 4.6.

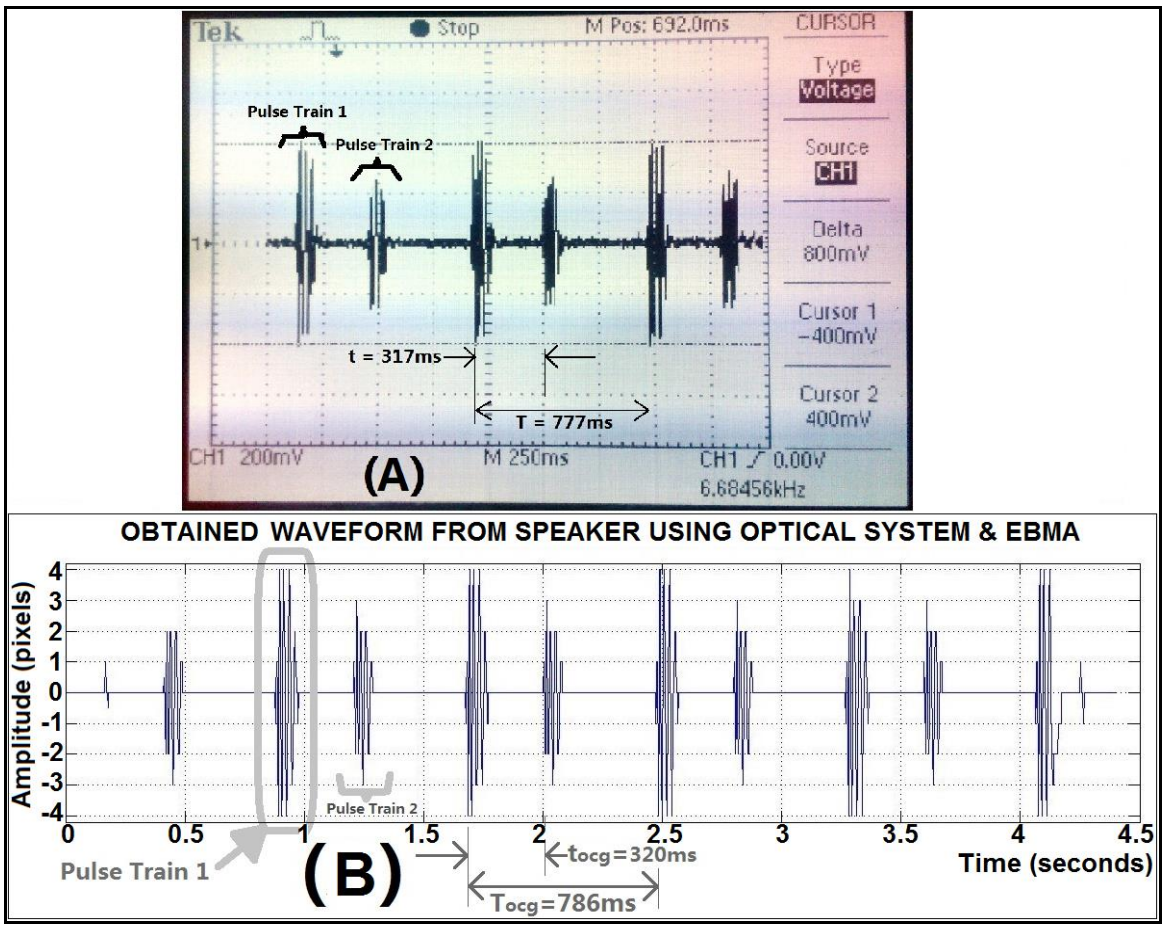

Fig. 4.5 (A): Oscilloscope display of the waveform of the Heartbeat sound sent to the Speaker from the Laptop; (B): Optical Cardiogram-OCG or Temporal plot of the outcome from the Optical System and EBMA method, Tocg: OCG`s period, tocg: time interval in the OCG.

The exposure time was 661 us, and the frame rate was 500 fps. The Focus was 1.5 m, the aperture was 1, and focal length was 30 mm. The power of the Laser on the speaker was around 1.7 mW. A Heart Beat sound downloaded from internet [38] was reproduced in a laptop and its audio output was applied to the Speaker.

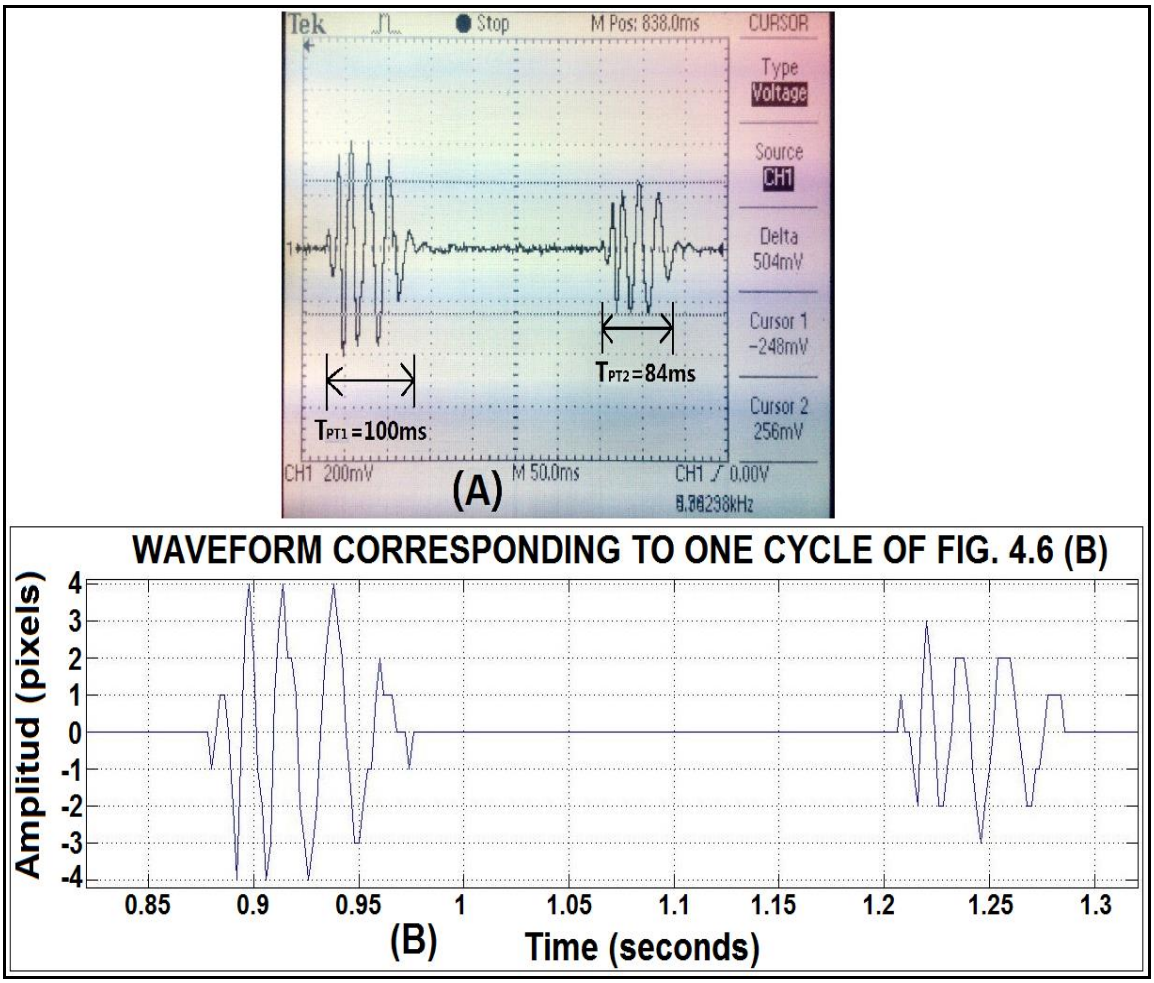

Fig. 4.6 (A): Oscilloscope display of one cycle of the waveform of the Heartbeat sound, T_{PT1} and T_{PT2} are the duration of Pulse Train 1 and Pulse Train 2 respectively [Fig 4.5]; (B): Temporal plot of the outcome from the Optical System and EBMA method corresponding to one cycle of the periodic waveform [Fig. 4.5 (B)].

At the same time, the audio output is measured by the Oscilloscope to compare with the wave which is obtained by the optical method and the EBMA.

The Fig 4.5 (A) shows a periodic Heartbeat wave where: Pulse Train 1 - PT1 has 0.8Vpp, Pulse Train 2 - PT2 has 0.504Vpp, a period T equal to 750ms, and an interval "t" between PT1 and PT2 equal to 317ms. The Fig 4.5 (B) shows a temporal plot or the OCG [cf. Chapter 1], which is very similar to the wave in (A), of the outcome of the EBMA method,

where: PT1 and PT2 have amplitudes peak to peak of 8 pixels and 6 pixels respectively, the period T_{ocg}=786ms and t_{ocg}=320ms which is the interval between PT1 and PT2. The amplitudes and the intervals in the Fig. 4.5 (A) and (B) are very similar, for example in PT1 the amplitude error is 0%, in PT2 the amplitude error is 19%, also the errors of T_{ocg} and t_{ocg} are 1.2% and 0.95% respectively. It should be noted that the errors have been calculated with the values obtained from the Oscilloscope.

The previous Fig. 4.6 shows one cycle of the temporal waveform corresponding to the Heartbeat sound presented in the Fig. 4.5. The Fig 4.6(A) and (B) are quite similar; in (B) the duration of PT1 and PT2 are 96.8ms and 80.7ms, with errors of 3.2% and 3.9% with respect to the durations T_{TP1} and T_{TP2} in (A).

4.3 Third Experiment: Measurement of BPP on Wrist

In this set of experiments the Laser beam was located on the wrist of the left arm of a person. The frame rate of the Camera was fixed at 100fps, Camera exposure was 500us, the focus was 10m, focal length was 30mm, and aperture was 1; the distance Camera/Laser to wrist was 50cm, the diameter of the Laser beam was 1mm, and the power of the Laser in a range from 0.6mW to 1.7mW.

Therefore $Z_2 = 9.5\text{m}$, $Z_3 = 10\text{m}$, $F = 30\text{mm}$, and $D = 1\text{mm}$.

A Digital Blood Pressure Monitor (DBPM) was used as a reference for the comparison with the results obtained by the Optical System and EBMA method. The following Fig 4.7 shows the arrangement of equipment and the location of one person.

For the measurements on the wrist, a small piece of double sided tape was adhered to the skin as a way to increase the reflection characteristics of the skin [39], the white release liner remained, and then the Laser beam was targeted on the white release liner tape.

During the measurements, the Laser was illuminated at the same place on the wrist, and the subjects kept their hands motionless. The Cuff of the DBPM was placed on the left arm.

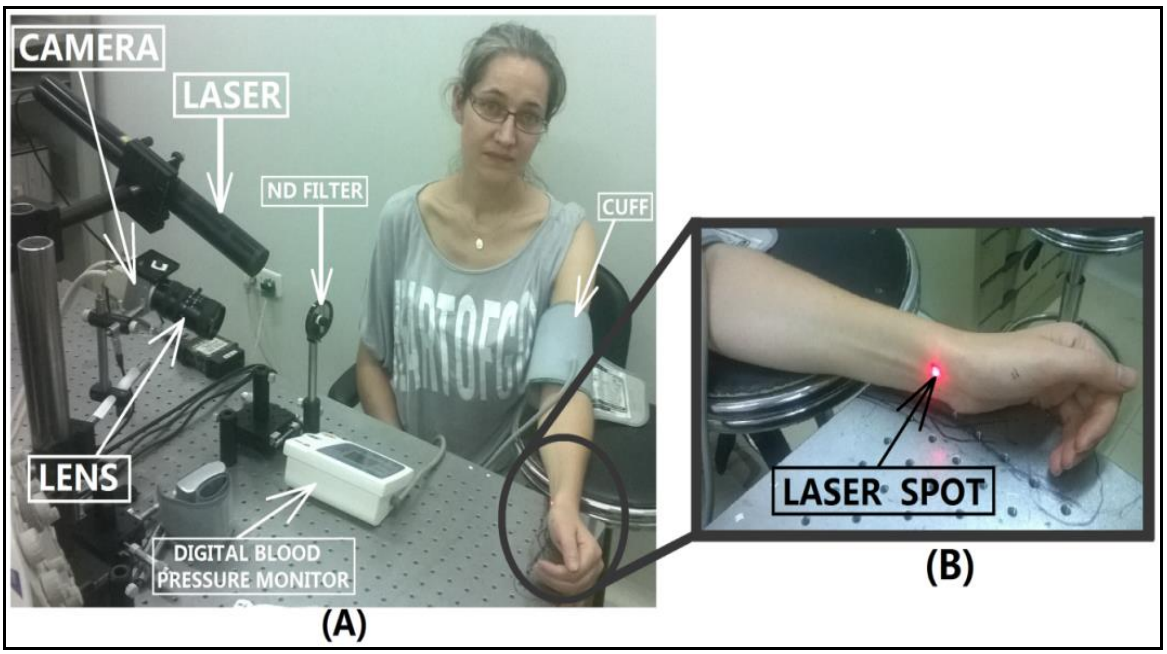

Fig. 4.7 (A): Setup of the experiment; (B): Wrist of the person where is shown the location of the laser spot on the radial artery.

There were 5 persons or subjects who participated in the experiments; the range of the age was 25-34 years old. The time for each measurement or trial was around 20 seconds for each subject; and right after, the DBPM was used to get the reference BPP. The sequence of the images obtained by the Camera were properly converted and processed in the Computer, and then the developed algorithm in this work which includes the EBMA method was used to process the frames of 64x64pixels. Finally the obtained values which are equivalent to the BPP were compared to the reference values obtained with the DBPM, where the BPP is the difference between SBP and DBP.

The measurements for the first four subjects denoted as: S1, S2, S3, and S4 were made when they were at rest, with seven trials for each of them; in regard of the fifth subject denoted as S5, twelve trials (S5-1 to S5-12) were made, where the S5-1 to S5-5 measurements were made when the subject was at rest and the S5-6 to S5-12 were made right after the subject made physical exercises (running at a good pace for 10 minutes).

Since the waveform obtained in this work, using the Optical System & EBMA method, is similar to the ECG but through optic means, as it is said before in the Chapter 1 (cf. Related work), that wave is called Optical Cardiogram (OCG) [1].

The laser power measured on the skin was less than 2mW, so still no special safety measures were required [40].

To get the Optical Method BPP [cf. Table 4.3] of one subject was made the following procedure:

a) For each trial, ten pulses were taken in the resultant OCG waveform.
b) For each pulse was calculated one maximum displacement *d* [cf. Fig. 4.9].
c) Then, for those ten pulses was calculated an average maximum displacement, this value was the Optical BPP of the trial.
d) Finally for the subject, the average of those Optical BPP values (amount of the values are the amount of trials) were calculated, this average became the Optical Method BPP of the subject.

To get the Digital Monitor BPP of one subject, the average of the differences between SBP and DBP measured by DBPM were calculated.

Below, the table 4.3 contains the final results of the measurements obtained using the Reference Monitor and the Optical System & EBMA method.

Table 4.3 General average results obtained by the Reference Monitor and the Optical System & EBMA method. BPP=Blood Pulse Pressure, HR=Heart Rate, bpm=beats per minute. Results are the average of the trials, and in the case of Optical Method BPP the value of each trial is the average of the first ten pulses.

SUBJECT	Number of Trials	Digital Monitor BPP (mmHg)	Optical Method BPP or *d* maximum (pixels)	Digital Monitor HR (bpm)	Optical Method HR (bpm)
S1/OCG-LMWLW	7	37.0	4.7	70	73
S2/OCG-LYLW	7	38.9	6.9	66	66
S3/OCG-HJYLW	7	38.9	6.2	75	81
S4/OCG-LYYLW	7	33.4	3.3	78	76
S5/OCG-RVLW	5	35.4	6.3	71	68

In the next Fig. 4.8 it is shown two images of the SP obtained by the Optical System corresponding to the sequence of images of the first trial of subject S5 (S5-1). A is the previous frame (first frame), B is the current frame (8^{th} frame), a block of 16x16 pixels in the

upper right part is marked with a rectangle, it can be seen in A that the block has "moved" 3 pixels up as indicated by the arrow in B.

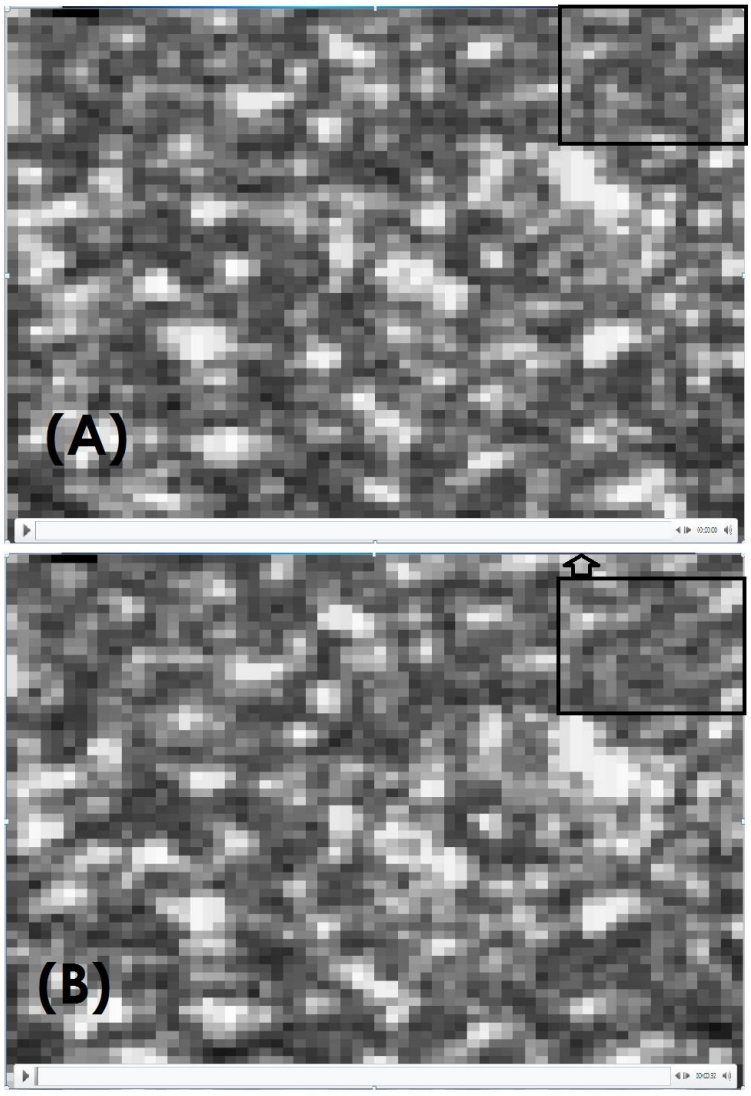

Fig. 4.8 Images of the moving Speckle Pattern (SP) of the subject S5-1. A is the SP at the time=0 second, B is the current SP at the time=0.07 seconds. The block of 16x16 pixels has moved 3 pixels up in A, which means the SP has moved 3 pixels up as well.

Fig. 4.9 shows the temporal plot for ten seconds of the OCG waveform from the first trial of the subject 5 which is S5-1, *d* maximum is indicated in the chart above, Fig. 4.9 also shows the amplitude spectrum with axe X in beats per minute (bpm), the spectrum shows that the HR was 72 bpm which was exactly the same value obtained by the Reference Monitor.

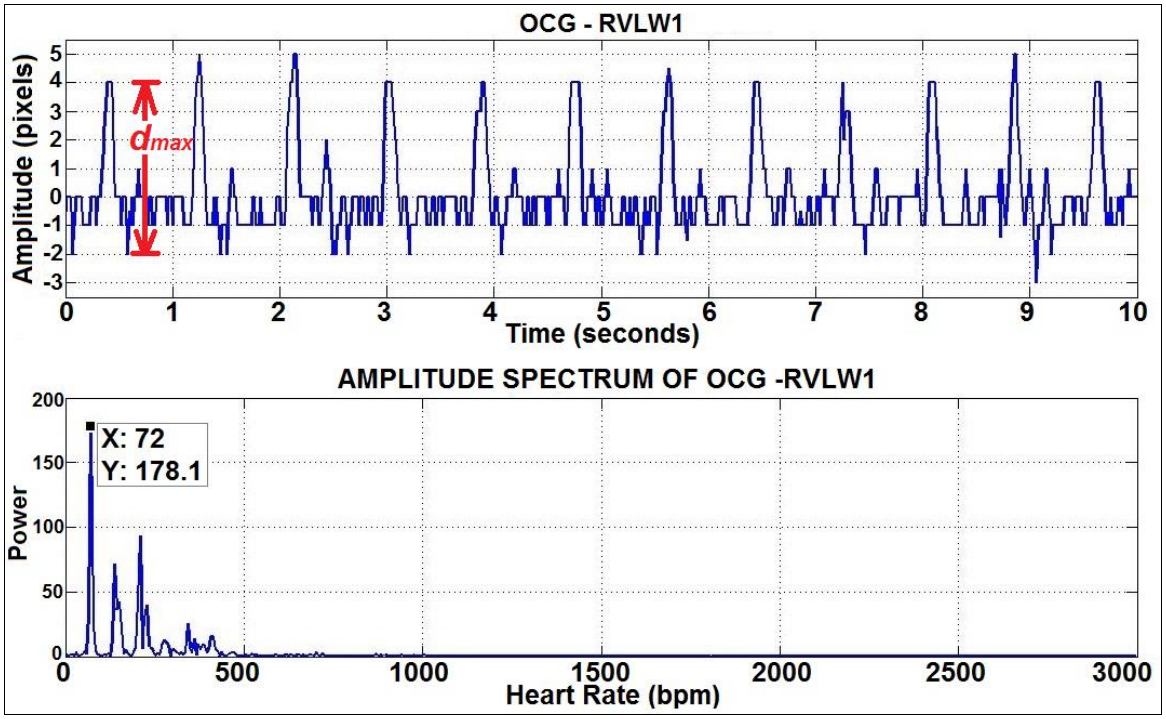

Fig. 4.9 Experimental results from the Optical System and EBMA method for the fifth subject in its first trial (S5-1), the subject was at rest. The chart above is the temporal plot of the outcome, i.e. it is the OCG, which is the amplitude of the relative shift of the SP between two subsequent frames; the chart below is its amplitude spectrum where the unit of the axis X is "Heart Rate" in bpm.

In order to calculate the maximum alpha angle (α_{max}) of the tilting movement of the skin in the wrist for this experiment, I replaced $Z_2 = 9.5$m, Z_3=10mA, F=30mm, and the values d maximum from the previous Table 4.3 in the Eq. 2.24 for each participant. The results are shown in the following Table 4.4.

Table 4.4 Values of the maximum tilt angle (α_{max}) of the skin on the wrist, corresponding to the maximum displacement d from the Table 4.3. These values were calculated using the Eq. 2.24.

Subject	S1	S2	S3	S4	S5
α_{max} (degrees)	0.131	0.194	0.173	0.093	0.177

The next Fig. 4.10 shows the OCG for each participant S1 to S5 corresponding to an interval of 10 seconds.

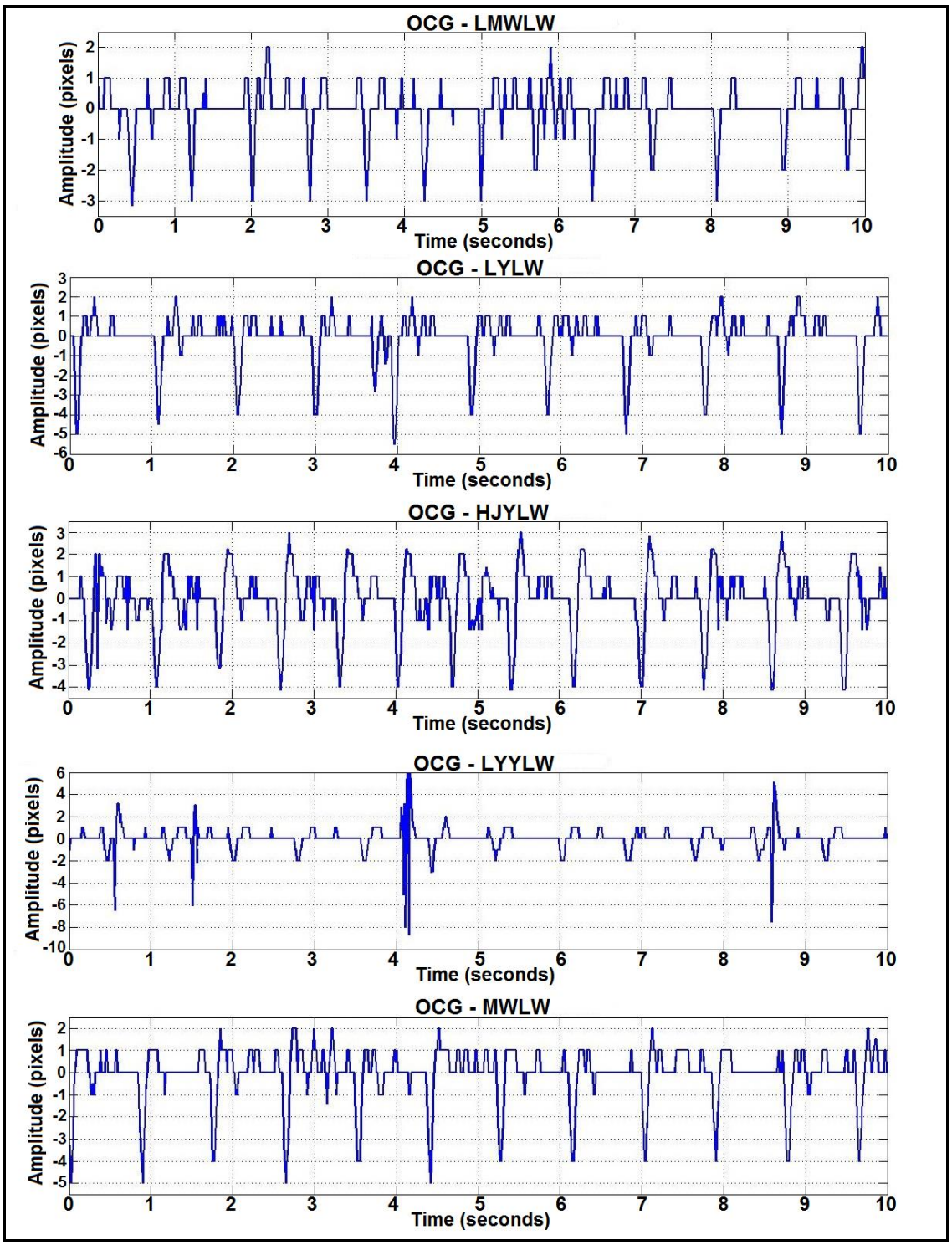

Fig. 4.10 Experimental results for the participants S1 to S5, up to down respectively, at rest. The charts are the temporal plot of the outcome, i.e. they are the OCG.

Next, the Fig 4.11 shows the OCGs for two trials of the subject S5 (sixth trial or OCG-RVLW6 and twelfth trial or OCG-RVLW12), right after exercise, it can be seen the

notorious difference between them in amplitude and period, with higher amplitude and shorter period in S5-12.

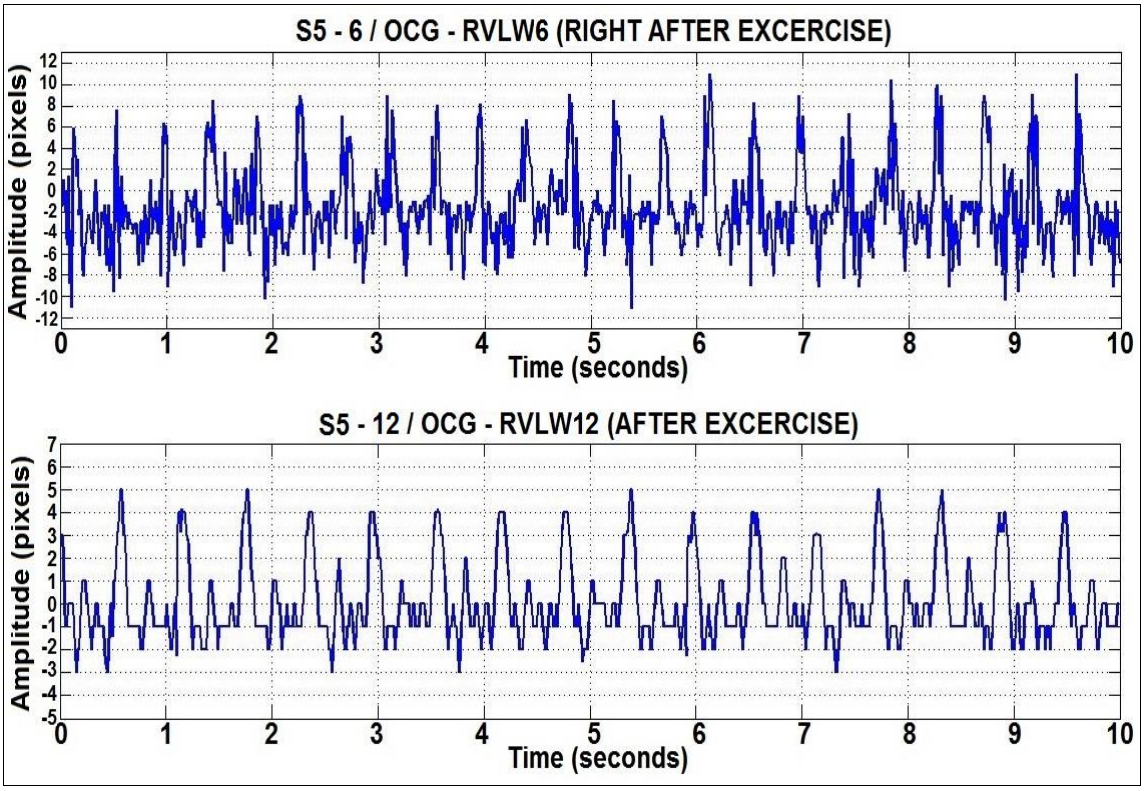

Fig. 4.11 Experimental results for the participant S5. The chart above and the one below are for S5-8 and S5-14 respectively, the subject was at the state right after physical exercises.

The extracted results (Optical Method BPP or *d* maximum – Table 4.3) with the Optical System & EBMA method were compared with reference measurements (Digital Monitor BPP – Table 4.3) obtained by conventional means (DBPM), the result of this comparison is shown in the next Fig. 4.12. It shows a linear relation between them and a correlation coefficient equal to 0.76.

The next table 4.5 contains the numerical values of the obtained results for the Subject S5 right after exercise. This table also shows the maximum tilt angle α_{max} and the value of the pressure after applying the linear scale factor in order to convert units of pixels to units of blood pressure. The linear scale factor will be discussed below.

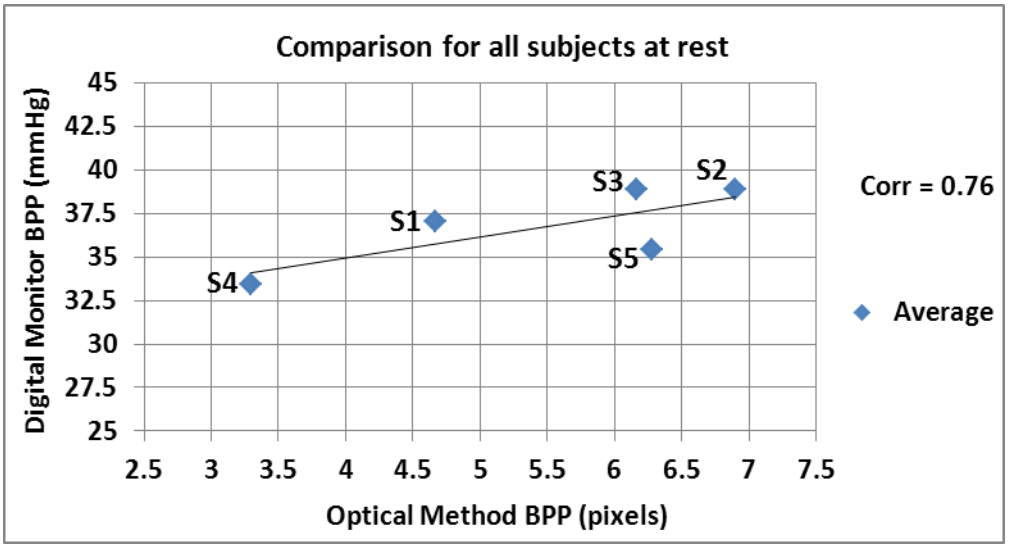

Fig. 4.12 Comparison of the obtained values between Reference Monitor (Digital Monitor) and Optic System & EBMA Method (Optical Method) for all the subjects from the experimental results in Table 4.3.

Table 4.5 Results for the participant S5 right after exercise, the obtained scaling factor in the Fig. 4.13(A) was applied to the value of the Optical Method BPP, to convert the pixels units to mmHg units. The maximum tilt angle α_{max} was calculated using the Eq. 2.24.

TIME (minutes)	Digital Monitor BPP (mmHg)	Optical Method BPP or *d* maximum (pixels)	Optical Method BPP with scaling factor - linear fit curve (mmHg)	α_{max} (degrees)
0	69	16.5	69.5	0.463
4	50	9.2	43.5	0.258
7	41	10.3	47.4	0.289
12	43	7.9	38.8	0.221
17	46	9.0	43.0	0.254
30	30	6.8	35.0	0.191
36	33	6.7	34.8	0.189

This table shows that the maximum angle obtained for the sixth trial of subject S5 was 0.463 degree.

To calculate the resolution of the system implemented in this work, i.e. to calculate the minimum angle that the system can detect, I replaced the parameters $Z_2 = 9.5\text{m}$, $Z_3 = 10\text{mA}$, $F = 30\text{mm}$ in the Eq. 2.24, and taking into account that the minimum detected movement in

the camera sensor with EBMA method was one pixel, which means d = 1, the result showed that the resolution of the System was 0.028 degrees.

Then, the Fig. 4.13 shows the comparison of the experimental results for only the participant S5 right after exercise; the chart (A) shows a linear relation between them with a correlation coefficient equal to 0.93; the chart (B) shows the plot in the time of the experimental results from the Table 4.5, the Optical Method BPP is scaled to the values of pixels and to the values of pressure, where a scaling factor was chosen to match two different dimensions estimated by the system and manually measured values, the scaling factor was the linear fit curve showed in the chart (A): $y = 3.5639x + 10.797$, the obtained values are shown in the Table 4.5.

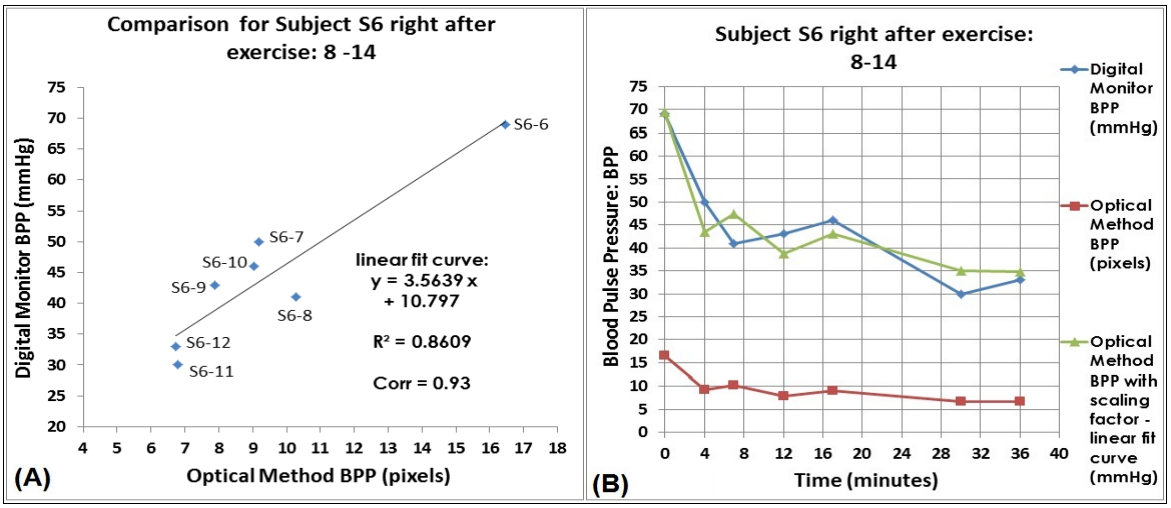

Fig. 4.13 Results for the participant S5 right after exercise: The chart (A) is the comparison between the experimental results, the chart (B) shows the matching between the Optic System & EBMA method measurements obtained and the reference measurement obtained using the Blood Pressure Monitor. Both charts based in the Table 4.3.

4.4 Fourth Experiment: Measurement of BPP on Cubital Fossa

In this experiment, with the Optical System and EBMA method, the BPP on the median cubital vein in the cubital fossa of the left arm (cf. Figure 4.14) was measured at the same time that blood pressure was measured with the conventional system, with the cuff placed around the upper of the left arm as well. The aim of this experiment was to see how the BPP varies in the vein close to the Cuff during a conventional blood pressure measurement; the same Blood Pressure Monitor of the previous experiment was used.

A sixth subject S6 participated in the experiment, the BPP was measured during 46 seconds in order to cover the time of measurement using the monitor, which was about 38 seconds for the subject S6. Then, the resultant OCG, the X axe OCG and the variation of BPP for each pulse was plotted. The result is shown in the Fig. 4.15.

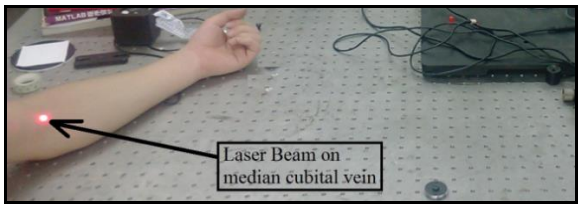

Fig. 4.14 Laser Beam to measure BPP on Median Cubital Vein in the Cubital Fossa, near the location of the Cuff.

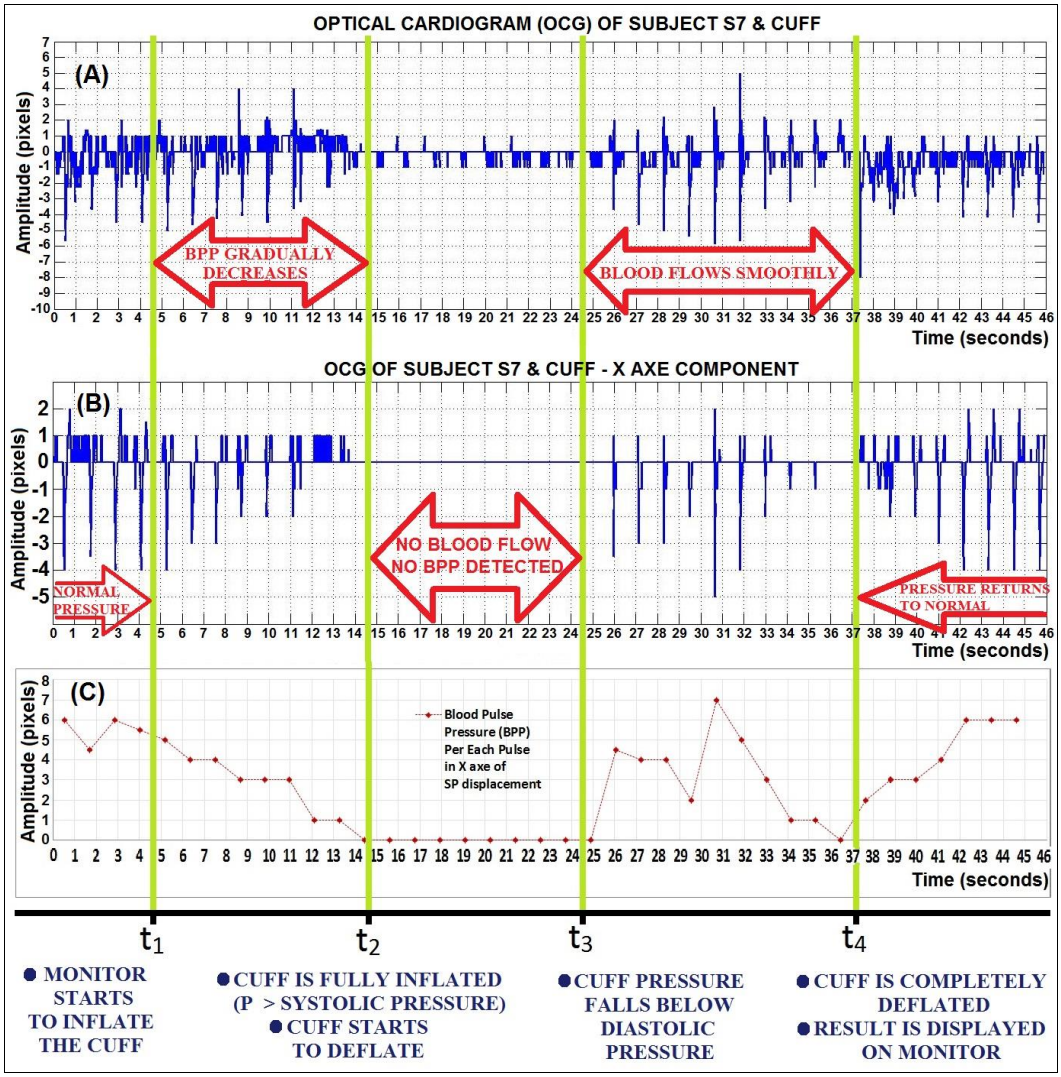

Fig. 4.15 Experimental results for the participant S6 at rest: Chart (A) is the resultant OCG, Chart (B) shows the X axe OCG, and Chart (C) shows the BPP.

The meaning of the noted times and intervals in the Fig. 4.15 and a brief analyze of them are as follows [41]:

1) t_1 : The monitor starts to inflate the cuff on the upper arm.
2) t_1 - t_2 : The BPP gradually decreases, from normal to zero.
3) t_2 : The cuff is fully inflated to a pressure above the SBP, then the cuff starts to deflate.
4) t_2 - t_3 : No blood flow occurs through the vain, so no BPP detected (cf. Fig. 4.15 (A) and (C)).
5) t_3 : Cuff pressure falls below diastolic pressure of the subject S6.
6) t_3 - t_4 : Blood flows smoothly through the vein, so BPP is detectable.
7) t_4 : The cuff is completely deflated and the result is displayed on the monitor.

Referring to the third experiment, since the frame rate of the camera is 100fps, in 20 seconds were needed 2000 images for each measurement. According to the table 4.3, it was needed from 74 (60sec/81bpm x 100fps) images to 90 (60sec/66bpm x 100fps) images per pulse, which means that it was needed from 7.4 seconds to 9 seconds per ten pulses, sufficient time for the calculation of the average BPP.

5 Conclusion and Future work

5.1 Conclusions

The remote estimation method of blood pulse pressure and heart rate using speckles pattern tracking with exhaustive search block matching algorithm were presented in this work as well as their performance analysis.

The analysis showed that the remote estimation method enables the measurement of the frequency and amplitude of the signal driving of a speaker.

Furthermore, it also enables the measurement of people's blood pulse pressure and heart rate on an immobile wrist.

5.2 Future work

To avoid using tape stuck on the skin, further research could be conducted to add an appropriate data filter in the algorithm. Furthermore, in order to eliminate the effect of the patient's free movement and the translational and rotational laser-camera motions, it would be advisable to add video stabilization algorithms.

The results of this work could be implemented in an electronic-optical compact measurement system device that could measure the BPP, the HB and even the Respiration Rate without contact in real time, in the form of a portable device, which could include USB and Bluetooth connection, as well as show the respective waveforms on a digital display.

In regard to laser safety, since the laser should not be pointed directly at people's eyes, the device should be developed as class 1, enabling continuous monitoring of patients recovering in intensive care units, especially in preterm infants or in longer measurement time (case of hypertension), therefore the device will be convenient in the hospital environment.

Acknowledgment

I would like to hereby extend my special thanks to several people.

First, my supervisor Professor PhD Pengcheng Li, for his guidance, advices, patience and wisdom along this work. Also Professor Jinling Lu.

The staff of the International Students Office in Huazhong University of Science and Technology, and especially Mr. Ren who enabled me to prolong the time of my stay in China to finish this thesis.

My laboratory mates, especially Dong Wen, Jianjun Qiu, Jianyun Huang, Liangwei Meng, Miaowen Li, Ming Chen, Qin Huang, Yang Wang who helped me with the translation to Chinese of the Abstract, Yangyang Li, Ying Li, for their most useful help, advices, and participation in my experiments in the laboratory.

My family in Peru, especially my mother Teodora.

My friends from Holy Family Catholic Church, who supported me through encouragements and faithful prayers, especially Raphaëlle Vandermersch, Maire Larkin, Joe Houston, John Hamilton and John Shi.

Thank you, dear readers, for taking interest in my research.

Finally, I would like to give honor and thanks to the Holy Trinity: Father GOD, Son Jesus-Christ and Holy Spirit, for their endless mercy, faithfulness and love and to whom I owe everything about the accomplishment of this work. Amen. Alleluia!

Hugo Pumacahua Chahuayo
2014
In HUST

References

[1] Zalevsky, Z.,Garcia, J. Motion detection system and method. In Google Patents: 2014.

[2] Zalevsky, Z.,Beiderman, Y.,Margalit, I., et al. Simultaneous remote extraction of multiple speech sources and heart beats from secondary speckles pattern. Optics express, 2009, 17 (24): 21566-21580.

[3] Huang, Y.-H.,Ma, C.-C.,Chao, C.-K. High-frequency resonant characteristics of triple-layered piezoceramic bimorphs determined using experimental measurements and theoretical analysis. Ultrasonics, Ferroelectrics and Frequency Control, IEEE Transactions on, 2012, 59 (6): 1219-1232.

[4] Huang, Y.-H.,Ma, C.-C. Experimental and numerical investigations of vibration characteristics for parallel-type and series-type triple-layered piezoceramic bimorphs. Ultrasonics, Ferroelectrics and Frequency Control, IEEE Transactions on, 2009, 56 (12): 2598-2611.

[5] Tsutsumi, T.,Wakatsuki, D.,Shimojima, H., et al. Analyzing time-frequency power spectrum limited in QRS complex based on the wavelet transform. Int J Bioelectromagnetism, 2004, 6 (1): 25-32.

[6] Trägårdh, E., Schlegel, T. T. High‐frequency QRS electrocardiogram. Clinical physiology and functional imaging, 2007, 27 (4): 197-204.

[7] Bailey, J. J.,Berson, A. S.,Garson Jr, A., et al. Recommendations for standardization and specifications in automated electrocardiography: bandwidth and digital signal processing. A report for health professionals by an ad hoc writing group of the Committee on Electrocardiography and Cardiac Electrophysiology of the Council on Clinical Cardiology, American Heart Association. Circulation, 1990, 81 (2): 730.

[8] Optronis GmbH. Models of High-Speed cameras. http://www.optronis.com/en/products/high-speed-cameras/models.html

[9] Beiderman, Y.,Horovitz, I.,Teicher, M., et al. Remote estimation of blood pulse pressure via temporal tracking of reflected secondary speckles pattern. Journal of biomedical optics, 2010, 15 (6): 061707-061707-7.

[10] Nitzan, M.,Taitelbaum, H. The measurement of oxygen saturation in arterial and venous blood. Instrumentation & Measurement Magazine, IEEE, 2008, 11 (3): 9-15.

[11] Lokaj, P.,Parenica, J.,Goldbergova, M. P., et al. Pulse pressure in clinical practice. Eur J Cardiovasc Med, 2011, 2 (1): 66-68.

[12] Malone, A. F.,Reddan, D. N. Pulse pressure. Why is it important? Peritoneal Dialysis

International, 2010, 30 (3): 265-268.

[13] Singh, A.,Lubecke, V.,Boric-Lubecke, O. Pulse pressure monitoring through non-contact cardiac motion detection using 2.45 GHz microwave Doppler radar. In Engineering in Medicine and Biology Society, EMBC, 2011 Annual International Conference of the IEEE, 2011; 4336-4339.

[14] Lin, H.-D.,Lee, Y.-S.,Chuang, B.-N. Using dual-antenna nanosecond pulse near-field sensing technology for non-contact and continuous blood pressure measurement. In Engineering in Medicine and Biology Society (EMBC), 2012 Annual International Conference of the IEEE, 2012; 219-222.

[15] Wang, C.,Trivedi, S. B.,Jin, F., et al. Human life signs detection using high-sensitivity pulsed laser vibrometer. IEEE Sensors Journal, 2007, 7 (9/10): 1370.

[16] Kaplan, A. D.,OrSullivan, J. A.,Sirevaag, E. J., et al. Hidden state models for noncontact measurements of the carotid pulse using a laser doppler vibrometer. Biomedical Engineering, IEEE Transactions on, 2012, 59 (3): 744-753.

[17] Gyaourova, A.,Kamath, C.,Cheung, S. Block matching for object tracking. Lawrence livermore national laboratory, 2003.

[18] Chitaliya, N.,Trivedi, A. Novel block matching algorithm using predictive motion vector for video object tracking based on color histogram. In Electronics Computer Technology (ICECT), 2011 3rd International Conference on, 2011; 81-85.

[19] Sugandi, B.,Kim, H.,Tan, J. K., et al. A Block Matching Technique for Object Tracking Based on Peripheral Increment Sign Correlation Image. In InTech: 2011.

[20] Cheung, C.-H.,Po, L.-M. Novel cross-diamond-hexagonal search algorithms for fast block motion estimation. Multimedia, IEEE Transactions on, 2005, 7 (1): 16-22.

[21] Barjatya, A. Block matching algorithms for motion estimation. IEEE Transactions Evolution Computation, 2004, 8 (3): 225-239.

[22] Pandian, S.,Bala, G. J.,George, B. A. A Study on Block Matching Algorithms for Motion Estimation. International Journal on Computer Science & Engineering, 2011, 3 (1).

[23] Manap, R.,Ranjit, S.,Basari, A. A., et al. Performance Analysis of Hexagon-Diamond Search Algorithm for Motion Estimation. In Computer Engineering and Technology (ICCET), 2010 2nd International Conference on, 2010; V3-155-V3-159.

[24] Tourapis, A. M.,Au, O. C.,Liou, M. L. Highly efficient predictive zonal algorithms for fast block-matching motion estimation. Circuits and Systems for Video Technology, IEEE Transactions on, 2002, 12 (10): 934-947.

[25] Mahmoud, H.,Goel, S.,Shaaban, M., et al. A new efficient block-matching algorithm for

motion estimation. Journal of VLSI signal processing systems for signal, image and video technology, 2006, 42 (1): 21-33.

[26] Santamaria, M.,Trujillo, M. A comparison of block-matching motion estimation algorithms. In Computing Congress (CCC), 2012 7th Colombian, 2012; 1-6.

[27] Po, L.-M.,Ng, K.-H.,Wong, K.-M., et al. Multi-direction search algorithm for block-based motion estimation. In APCCAS, 2008; 1466-1469.

[28] Po, L.-M.,Ng, K.-H.,Cheung, K.-W., et al. Novel directional gradient descent searches for fast block motion estimation. Circuits and Systems for Video Technology, IEEE Transactions on, 2009, 19 (8): 1189-1195.

[29] Beiderman, Y.,Blumenberg, R.,Rabani, N., et al. Demonstration of remote optical measurement configuration that correlates to glucose concentration in blood. Biomedical optics express, 2011, 2 (4): 858-870.

[30] Scalise, L. Non contact heart monitoring. Advances in Electrocardiograms-Methods and Analysis. InTech. ISBN, 2012, 978-953.

[31] Sirohi, R. Optical methods of measurement: wholefield techniques. CRC Press, 2010.

[32] Rabal, H. J.,Braga Jr, R. A. Dynamic laser speckle and applications. CRC Press, 2010.

[33] Lipson, A.,Lipson, S. G.,Lipson, H. Optical physics. Cambridge University Press, 2010.

[34] Gao, E.,Young, W. L.,Ornstein, E., et al. A theoretical model of cerebral hemodynamics: application to the study of arteriovenous malformations. Journal of Cerebral Blood Flow & Metabolism, 1997, 17 (8): 905-918.

[35] Wang, Y.,Ostermann, J.,Zhang, Y.-Q. Video processing and communications. Prentice Hall Upper Saddle River, 2002.

[36] Tintaya, C. O. J. PROCESAMIENTO DIGITAL DE SEÑALES SISMICAS EN ENTORNO MATLAB.

[37] Beiderman, Y.,Amsel, A. D.,Tzadka, Y., et al. A microscope configuration for nanometer 3-D movement monitoring accuracy. Micron, 2011, 42 (4): 366-375.

[38] 3M. Heart Sounds. http://int-prop.lf2.cuni.cz/heart_sounds/h15/sounbody.html (June 20),

[39] Scalise, L.,Ercoli, I.,Marchionni, P., et al. Measurement of respiration rate in preterm infants by laser Doppler vibrometry. In Medical Measurements and Applications Proceedings (MeMeA), 2011 IEEE International Workshop on, 2011; 657-661.

[40] UCSB Environmental Health & Safety. Laser Safety Manual. In.

[41] Lopez, S. Blood Pressure Monitor Fundamentals and Design. 2012.